



Contents lists available at ScienceDirect

Deep-Sea Research II

journal homepage: www.elsevier.com/locate/dsr2

On the characteristics of internal tides and coastal upwelling behaviour in Marguerite Bay, west Antarctic Peninsula

Margaret I. Wallace^{a,*}, Michael P. Meredith^b, Mark A. Brandon^c, Toby J. Sherwin^d, Andrew Dale^d, Andrew Clarke^b

^a Gatty Marine Research Institute, University of St Andrews, St Andrews, KY16 8LB, UK

^b British Antarctic Survey, High Cross, Madingley Road, Cambridge CB3 0ET, UK

^c Centre for Earth, Planetary, Space and Astronomical Research, The Open University, Walton Hall, Milton Keynes MK6 7AA, UK

^d The Scottish Association for Marine Science, Dunstaffnage Marine Laboratory, Oban, Argyll PA37 1QA, UK

ARTICLE INFO

Article history:

Accepted 21 April 2008

Available online 5 August 2008

Keywords:

Coastal upwelling

Internal tides

Sea ice

Antarctic Peninsula

Marguerite Bay

ABSTRACT

Internal waves and coastal upwelling have important roles in both physical oceanography and marine ecosystems, via processes such as mixing of water masses and transfer of heat and nutrients to biologically active layers. In this paper we use quasi-weekly hydrographic profiles and moored records of temperature, salinity and water velocity to investigate the nature of internal tides and coastal upwelling behaviour in northern Marguerite Bay at the western Antarctic Peninsula. Within Ryder Bay, a near-coastal site in northern Marguerite Bay, atmospherically forced oscillations of the water column with periods around 2–7 days are observed, associated with wind-induced coastal upwelling and downwelling. Sea-ice cover is seen to play a role in the seasonal suppression of these oscillations. Significant internal tides also are observed at this site. A range of processes are seen to be important in controlling internal tide variability, including changes in local stratification and sea-ice conditions. Both diurnal and semidiurnal internal tidal species are observed, despite the study region being poleward of the critical latitude for diurnal internal tides. This suggests that at least the diurnal internal tides are generated close to the study location, and we investigate likely sources.

© 2008 Elsevier Ltd. All rights reserved.

1. Introduction

Both ocean upwelling and internal gravity waves are key phenomena in physical oceanography and have an impact upon marine ecology. Coastal upwelling and downwelling arise predominantly as a result of alongshore wind stress and the divergence of Ekman transport at the coast (Mitchum and Clarke, 1986), such that the tilt in the upwelled density structure is balanced by alongshore geostrophic flow. Coastal upwelling is predominantly an advective process that can lead to increased biological productivity, as the deep, upwelled waters are often nutrient-rich compared with those at the surface (e.g., Halpern, 1976; Winant, 1980; Small and Menzies, 1981). Conversely, downwelling has the potential to move biomass out of the light-favourable, shallow water environment, whilst both mechanisms can disrupt stable stratification via processes such as convection

and mixing, leading to low gradients in properties such as density, temperature, salinity and chlorophyll.

Internal waves also can lead to mixing, particularly where interaction of the wave with topography leads to reflection and breaking, and potential redistribution of heat, salt and nutrients. There has been significant work on the barotropic-to-baroclinic tidal energy transfer at fjord sills (see Stigebrandt, 1999, for a review), and numerous studies have concluded that the vertical mixing and circulation in fjords is predominantly driven by such processes (e.g., Stigebrandt, 1976; Stigebrandt and Aure, 1989; Simpson and Rippeth, 1993). The interaction between internal waves and the seabed may induce wave breaking, the formation of local regions of high shear, and enhanced turbulence; these lead to dissipation of the internal wave energy (e.g., Polzin et al., 1997). Similar processes have been observed on the continental shelf (New, 1988; Sherwin, 1988; New and Pingree, 1990; Rippeth and Inall, 2002), whilst diapycnal mixing in the deep ocean away from topography is also driven predominantly by internal wave activity (Munk and Wunsch, 1998). Internal tides have been observed in both the Arctic (Konyaev et al., 2000; Konyaev, 2000; Morozov et al., 2003) and the ocean close to Antarctica (Foldvik et al., 1990; Levine et al., 1997; Albrecht et al., 2006), and modelling work has

* Corresponding author. Tel.: +44(0) 1334 463513; fax: +44(0) 1334 463443.

E-mail addresses: miw5@st-andrews.ac.uk (M.I. Wallace), mmm@bas.ac.uk (M.P. Meredith), m.a.brandon@open.ac.uk (M.A. Brandon), Toby.Sherwin@sams.ac.uk (T.J. Sherwin), Andrew.Dale@sams.ac.uk (A. Dale), accl@bas.ac.uk (A. Clarke).

suggested that these features are locally generated via the interaction of barotropic tides with seabed topography (e.g., Morozov and Pisarev, 2002; Padman et al., 2006). However, the role of internal tides in mixing is not well constrained, and studies have shown that tidally induced mixing can be small, even in the presence of energetic baroclinic tides (Muench et al., 2002; Padman et al., 2006).

Internal waves can arise from a number of sources, including the interaction of currents, such as barotropic tides and wind-induced flows, with seabed topography (e.g., New, 1988; Stigebrandt, 1999; Levine et al., 1997). Once generated, linear wave theory predicts that freely propagating waves are restricted to a frequency, ω , where $f^2 < \omega^2$, and f is the inertial frequency (LeBlond and Mysak, 1978). Thus, for any wave with a period greater than 12 h, there is a critical latitude beyond which it cannot propagate freely because its frequency is less than f . In reality, seabed topography disrupts this simple theory (LeBlond and Mysak, 1978), and internal waves can be generated poleward of the critical latitude and propagate along a bathymetric barrier (such as the coastline or a sloping bottom), confined to within approximately one internal Rossby radius of the barrier (Emery and Thomson, 2004). The critical latitude for a diurnal internal tide is 30° in both hemispheres, whilst those for the M2 and S2 semidiurnal internal tides are 75° and 85° , respectively, placing all polar oceans beyond the critical latitude for diurnal internal tides and some beyond those for semidiurnal internal tides. Here, we investigate observations of both internal tides and atmospherically forced coastal upwelling/downwelling in Marguerite Bay, west Antarctic Peninsula, between January 2005 and April 2007.

2. Western Antarctic Peninsula shelf waters

The western Antarctic Peninsula (WAP) shelf (Fig. 1) is deep compared with most of the world's shelf seas (much of the shelf is 4–500 m deep), and features rough bathymetry and numerous deep troughs (≈ 1600 m) carved by glacial scouring. Offshore of the WAP shelf slope lies the southern boundary of the Antarctic

Circumpolar Current (ACC; e.g., Hofmann and Klinck, 1998; Klinck, 1998), which brings warm, saline circumpolar deep water (CDW) close to the slope, from where it can access the shelf (Martinson et al., 2008). The glacial troughs are preferential routes for this intrusion of CDW, and the less-dense variety of this water mass (upper CDW; UCDW) in particular accesses the shelf via this route (Klinck et al., 2004). Above UCDW lies the seasonally varying Antarctic Surface Water (AASW), which is separated from the underlying waters by a permanent pycnocline at 150–200 m (Beardsley et al., 2004; Hofmann and Klinck, 1998; Smith et al., 1999). The depth of this boundary is linked to sea-ice conditions, with a generally deeper pycnocline in years with sea-ice production greater than the temporal mean (Smith and Klinck, 2002; Meredith et al., 2004). Vertical transfer of heat across the pycnocline from the UCDW to AASW leads to relatively low rates of sea-ice production in the area, ensuring that surface waters under present climate conditions do not become denser than the underlying modified UCDW and thereby prohibiting the formation of dense deep and bottom waters (Martinson et al., 2008). During winter, pack ice covers the shelf and the surface layer is uniformly mixed to 100 m depth or more, with water at or near the freezing point (temperature, T , $\approx 1.8^\circ\text{C}$) (Smith et al., 1999; Meredith et al., 2004). Salinity is increased via brine rejection during ice production, resulting in mixed-layer salinity, S , of approximately 34.1 during winter (Toole, 1981; Klinck et al., 2004). In summer, shallow surface layers (20–30 m) are refreshed by ice melt and warmed by solar heating; these overlie the remnant of the winter mixed layer, which is now termed Winter Water (WW). This persists during summer as a relative vertical minimum in temperature at 70–100 m (Klinck, 1998; Klinck et al., 2004), though occasionally as deep as 150 m (Meredith et al., 2004). Over summer and autumn, increased storm activity leads to the breakdown of these layers and remnant WW undergoes mixing with surface and subpycnocline waters, leading to erosion of the WW signature in areas such as Ryder Bay (Meredith et al., 2004). This does not appear to be a shelf-wide process, however, as data from west of Adelaide Island show the presence of the typical WW minimum well into autumn (Klinck et al., 2004).

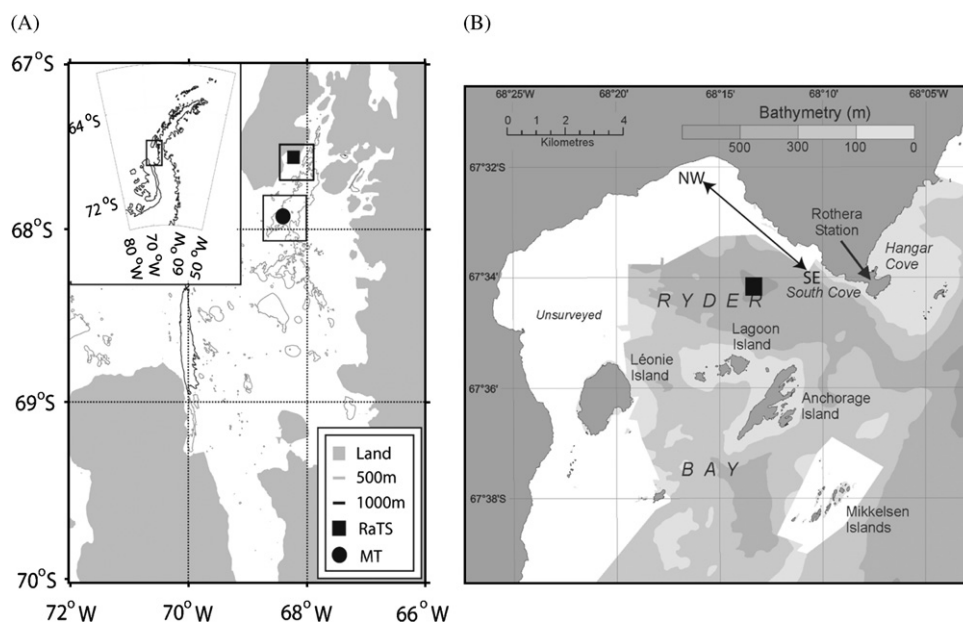


Fig. 1. (A) Marguerite Bay (black box on inset of the Antarctic Peninsula). The coast, 1000 m contour and 500 m contours are delineated by thick grey, thin black and thin grey lines, respectively. The RaTS mooring (black square) and the MT mooring (black circle) are shown, and thick black lines delineate areas surrounding the moorings examined in Section 4.2. The area surrounding the RaTS mooring is expanded in (B), courtesy of the Mapping and Geographic Information Centre (MAGIC), BAS. The RaTS site is marked with a black square. The black, double-headed arrow shows the NW–SE wind orientation to which Section 4.1 refers.

On the WAP shelf, UCDW intrusions mix with AASW to produce modified UCDW, which has properties intermediate between the two water masses, and are thus crucial for the heat and salt budgets of the region (Hofmann and Klinck, 1998; Klinck, 1998; Smith et al., 1999; Smith and Klinck, 2002; Martinson et al., 2008). Several studies suggest that internal wave activity and localised mixing over the rugged topography may play a role in this process (Klinck, 1998; Smith and Klinck, 2002; Dinniman and Klinck, 2004), whilst Howard et al. (2004) concluded that coastal upwelling could be a significant factor contributing to the upward flux of UCDW properties and has the potential to raise UCDW into the depth range affected directly by surface stress. The role of these processes in mixing is the subject of ongoing investigations.

Due to its high primary productivity, the WAP continental shelf supports a large biomass of Antarctic krill (Ross et al., 1996a), and consequently large populations of higher predators such as penguins (Fraser and Trivelpiece, 1996) and seals (Costa and Crocker, 1996). This biological productivity is strongly linked to physical processes (Ross et al., 1996b), so internal wave- or upwelling-induced disruption of stratification, both of which influence nutrient and phytoplankton distribution (Small and Menzies, 1981; Ostrovsky et al., 1996; Mackinnon and Gregg, 2005), have the potential to affect the entire marine ecosystem of the region. Such mixing is also known to influence the redistribution of heat in the upper ocean (Gregg, 1987; Mackinnon and Gregg, 2005; Winant, 1980), which has the potential to influence sea-ice conditions, whilst tidally forced currents are known to influence sea-ice conditions via processes such as lead formation (Kowalik and Proshutinsky, 1994; Koentopp et al., 2005). Therefore, both coastal upwelling/downwelling and internal wave activity can be expected to have a significant impact upon a seasonally sea ice-covered region of high biological productivity such as Marguerite Bay. In this paper we investigate these phenomena, using a combination of observational data and theoretical considerations.

3. Methods

To investigate internal wave and coastal upwelling activity in northern Marguerite Bay we use two data sources. The first is part of the British Antarctic Survey's Rothera Biological and Oceanographic Time Series Study (RaTS; Clarke et al., 2008). As part of RaTS, a year-round time series of conductivity–temperature–depth (CTD) profiles from a nearshore location in Ryder Bay (a small embayment at the northern end of Marguerite Bay; 67°13.20'S, 68°11.50'W; 520 m water depth; Fig. 1) has been collected since 1998. These data have been supplemented in recent years by our second source of data: fixed moorings at both the RaTS site (location above) and an offshore location in a deep glacial trough on the WAP continental shelf (67°15.39'S,

68°12.15'W; 840 m water depth; Fig. 1). This trough lies off the main axis of Marguerite Trough and the mooring is hereafter referred to as MT. In this paper, we focus on data from the quasi-weekly RaTS CTD casts in conjunction with moored CTD, temperature–depth recorder (TDR), temperature recorder (TR) and Acoustic Doppler Current Profiler (ADCP) time series from both moorings.

Moored data are summarised in Table 1 and were collected from the RaTS site for January 2005–April 2007 (three consecutive deployments) over the depth range 0–280 m, and from MT for January 2005–2006 (one deployment) over the depth range 0–564 m. In this paper, we refer to each RaTS mooring deployment by its number within the sequence (1, 2 or 3), the timings of which are detailed in Table 1. A delay in the intended recovery and redeployment of the moorings in January 2006 led to a data gap of roughly 3 weeks in all sensors except the ADCPs, which had sufficient onboard data storage to allow uninterrupted collection up to recovery in mid-February. The MT mooring was lost during the second deployment, hence the collection of only 1 year of data at this site.

The moored CTDs, TDRs and TRs were manufactured by Richard Brannckner Research (RBR) Ltd, and were configured to collect data at hourly intervals, whilst the 75 kHz Workhorse Long Ranger ADCPs (RD Instruments) averaged data into 15-min ensembles. At the RaTS site the RBR sensors were separated vertically by between 15 and 35 m within the depth range expected to sample modified UCDW (below 200 m). The upward-looking ADCP, at 200 m, measured the velocity profile of the upper water column with a vertical resolution of 4 m and a velocity resolution of 1 mm s⁻¹. At MT, the upward-looking ADCP (bin depth and velocity resolution as above), was located at 115 m, and the RBR sensors below 185 m at intervals of 50–70 m. Deployment depths and sample recording rates for each instrument are detailed in Table 2.

The CTD profiles at the RaTS site were carried out roughly 1–2 times per week from January 2005 to April 2007, using a SeaBird Electronics SBE-19 instrument. Deployment was from a small boat during the summer and through the sea-ice cover from a sledge during winter, given favourable ice conditions. Further details on data collection can be found in Meredith et al. (2004), Clarke et al. (2008) and Wallace (2007).

Surface meteorological data were obtained from Rothera Research Station, courtesy of the British Antarctic Survey. Hourly values of wind direction and speed were collected for three 30-day periods for the summer and winter of the first two RaTS mooring deployments and the summer of the third RaTS deployment. Linear interpolation was used to fill gaps in the wind time series, where not more than five consecutive data points were missing.

This analysis also makes use of the AntPen04.01 tide model (Padman, unpublished; www.esr.org/ptm_index), which is a high-resolution (1/301 longitude by 1/601 latitude, 2 km) forward model, based on the shallow water equations, and forced

Table 1
Deployment details for the Marguerite Bay moorings

Mooring	Water depth (m)	Deployment	Location (deg, min)	Deployed	Recovered	Deployment length (days)
RaTS	520	1	67°13.02'S 68°11.02'W	25/01/05	15/02/06	387
		2	67°13.97'S 68°11.06'W	17/02/06	16/12/06	3030
		3	67°13.01'S 68°11.00'W	17/12/06	09/04/07	114
MT	840	1	67°15.39'S 68°12.15'W	24/01/05	15/02/06	388

Table 2
Mooring configurations

Instrument	Sampling period	Deployment	Depth (m) [pressure (dbar)]
<i>RaTS site</i>			
CTD and 75 kHz ADCP	CTD: 1 h	1	200 [202]
	ADCP: 15 min ensembles	2	196 [199]
		3	195 [197]
TR	1 h	1	234
		2	228
		3	227
CTD	1 h	1	253 [255]
		2	244 [246]
		3	243 [245]
TDR	1 h	1	268 [271]
		2	259 [261]
		3	257 [260]
CTD	1 h	1	283 [286]
		2	274 [277]
		3	273 [276]
<i>MT site</i>			
CTD and 75 kHz ADCP	CTD: 1 h ADCP: 15 min. ensembles	1	114 [115]
TR	1 h	1	185
TDR	1 h	1	240 [242]
CTD	1 h	1	298 [302]
TR	1 h	1	352
TDR	1 h	1	406 [411]
CTD	1 h	1	457 [462]
TR	1 h	1	511
TDR	1 h	1	564 [571]

Abbreviations are as follows: CTD, conductivity–temperature–depth sensor; TDR, temperature–depth recorder; TR, temperature recorder; ADCP, Acoustic Doppler Current Profiler.

Depths of some instruments are approximate in the absence of pressure data.

at the open boundary by tide heights from the circum-Antarctic forward model (CATS02.01; Padman et al., 2002) and by astronomical forcing. The model is tuned to data using a linear benthic drag coefficient.

4. Results

Internal waves are observed in our data from Marguerite Bay at both diurnal and semidiurnal tidal frequencies, in addition to quasi-periodic fluctuations on timescales of a few days. The latter longer-period fluctuations appear to be atmospherically forced, and are investigated in Section 4.1, whilst the internal tides are explored in Section 4.2. Characteristic profiles of potential temperature, θ , S , potential density anomaly, σ_θ , and buoyancy frequency, N , from the RaTS site, along with a comparison of θ from the two mooring sites for the summers of 2005–2007 are shown in Fig. 2, and will be referred to throughout the following analyses. N is derived from the gravitational acceleration, g , the reference density at depth z , ρ_0 , and the vertical density gradient, $d\rho/dz$ (Pond and Pickard, 1983):

$$N^2 = -\frac{g}{\rho_0} \frac{d\rho}{dz} \quad (1)$$

4.1. Atmospherically forced fluctuations

Fig. 3 shows T , S and S_y time series from the RaTS site, along with the horizontal velocity from the ADCP bin immediately

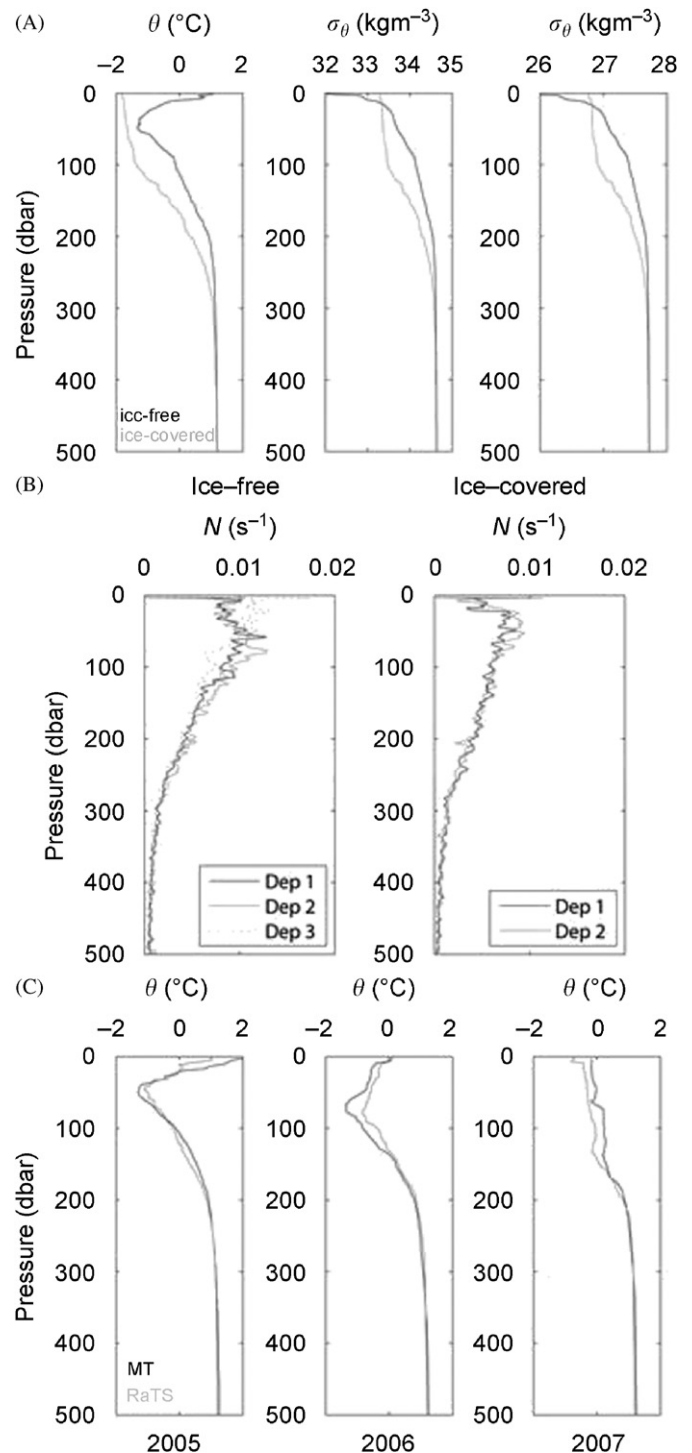


Fig. 2. (a) Typical profiles of potential temperature, salinity and potential density anomaly from the RaTS site for the ice-free (black) and ice-covered (grey) seasons. (b) Mean buoyancy frequency profiles for the ice-free and ice-covered seasons at the RaTS site (Dep 1–3 refer to the deployment). (c) Comparison of potential temperature profiles from the RaTS site (grey) and MT (black) from January 2005, February 2006 and April 2007.

below the surface, while Fig. 4 shows the corresponding T and ADCP data from the MT site. All time series are filtered using a 26-h Butterworth lowpass filter to remove tidal and higher frequency variability. Markedly low variance in the ADCP data is indicative of the presence of sea ice above the mooring (Visbeck and Fischer, 1995; Hyatt et al., 2008) and shaded in grey in Figs. 3

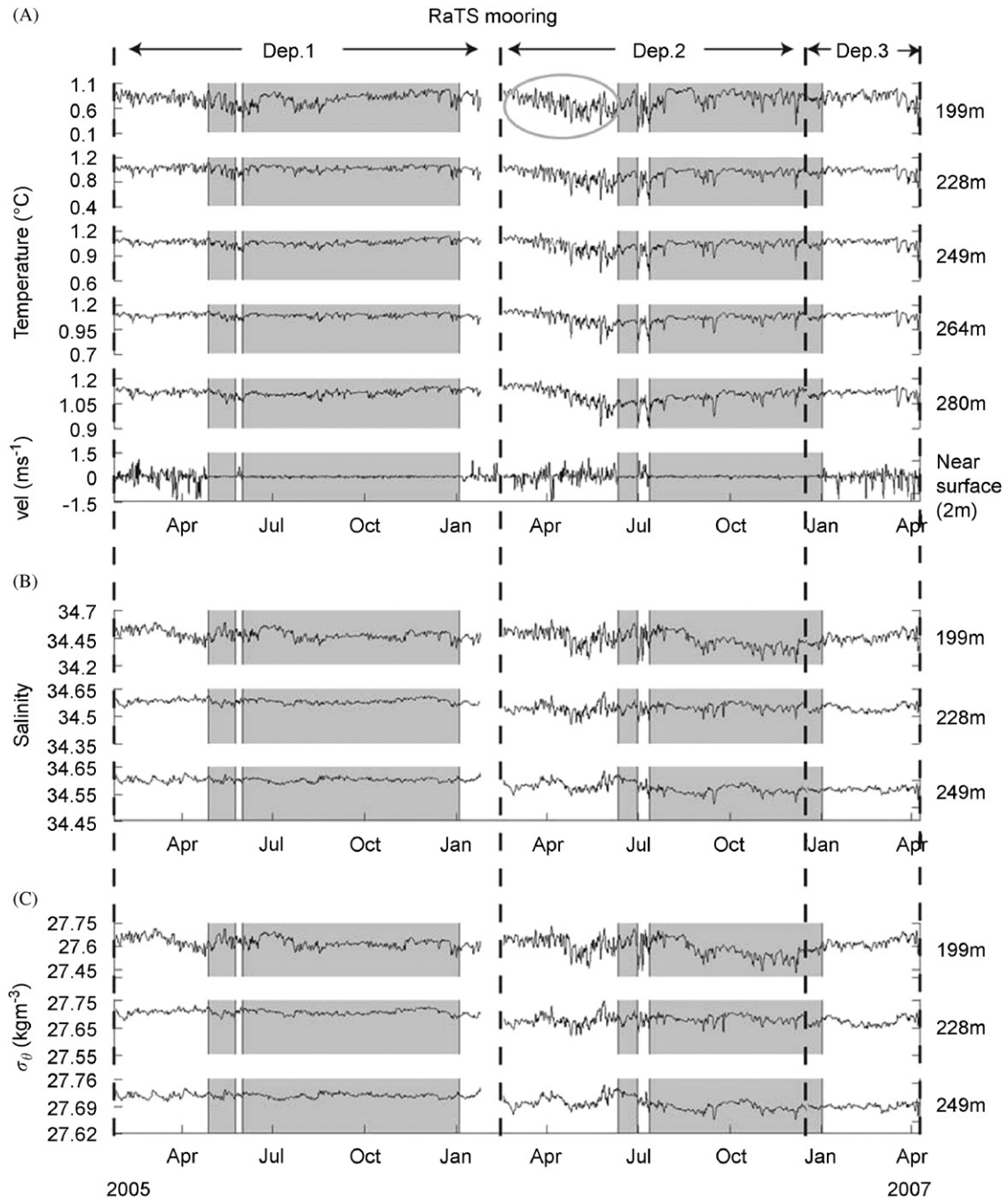


Fig. 3. (A) Temperature, T , (B) salinity, S , and (C) potential density anomaly, σ_θ , time series from the RaTS site. Horizontal velocity data from the bin of the upward-looking ADCP closest to the surface are included at the bottom of panel (A). All time series are filtered using a 26-h Butterworth lowpass filter to remove tidal and higher frequency variability. The velocity data are used to identify periods of ice cover (velocity variance is reduced in the presence of ice). Ice presence is shaded in grey on each panel. The three deployments are bordered by black dashed lines and the mean depth of each time series over the three deployments is noted to the right of each trace. The grey oval marks an example of the 2–7 days quasi-periodic signal examined in Section 4.1.

and 4. At the RaTS site in both 2005 and 2006 there were 3–4 weeks of ice cover, followed by 2–3 weeks of open water before the onset of pack ice. Ryder Bay may, in fact, be covered by fast ice for much of the winter, whilst the offshore regions of Marguerite Bay are covered in pack ice. Therefore, for simplicity, we will refer to all high concentration ice cover as ‘pack ice’. We term periods interpreted as being pack-ice covered as the ‘ice-covered season’, and periods of open water and those of brief ice cover the ‘ice-free season’.

Quasi-periodic fluctuations on timescales of 2–7 days have been observed in certain sections of the moored time series from

the RaTS site (an example of the signal is marked by the grey oval in Fig. 3), but are not observed at the MT mooring (Fig. 4). Their signal is variable both in magnitude and duration, and is observed in all of the RaTS temperature loggers (CTDs, TR, TDR), although the magnitude of the signal decreases with depth, which is consistent with the lower gradients observed deeper in the water column (Fig. 2). The fluctuations can also be seen in S and σ_θ at the uppermost CTD (199 m), but are more difficult to identify in these time series at the deeper sensors, due to lower signal-to-noise ratios compared with those in T (Wallace, 2007). Thus, our analysis will concentrate upon T data. The thermohaline

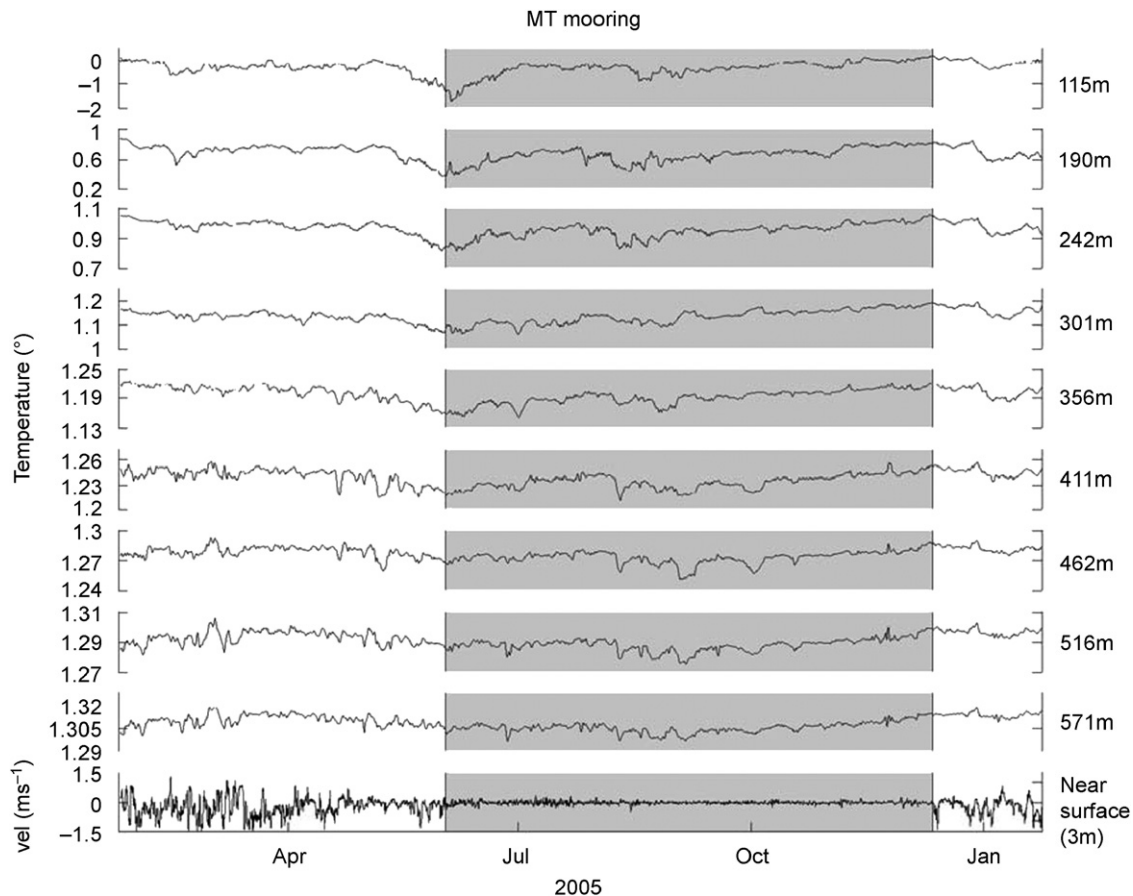


Fig. 4. Temperature time series from the MT site. Horizontal velocity data from the bin of the upward-looking ADCP closest to the surface are included at the bottom of the panel. All time series are filtered using a 26-h Butterworth lowpass filter to remove tidal and higher frequency variability. The velocity data are used to identify periods of ice cover (velocity variance is reduced in the presence of ice). Ice presence is shaded in grey on each panel. The depth of each time series is noted to the right of each trace.

properties of UCDW are relatively invariant (Hofmann and Klinck, 1998; Wallace, 2007), and at the RaTS site temperature below the WW minimum at the RaTS site consistently increases with depth (Meredith et al., 2004; Wallace, 2007). Thus, for this location, and for our specific purposes, isotherms can be considered analogous to isopycnals in UCDW and T can reasonably be considered a proxy for S_y , allowing more complete coverage of the water column than density time series would allow.

The fluctuations are apparently unaffected by the initial periods of ice cover, but are smaller in magnitude in the presence of pack ice. A high degree of interannual variability is also observed, with the fluctuations being most pronounced in February–June during deployment 2 (2006). Although reduced during the ice-covered season, the signal is clearly visible during 2006, whereas during 2005 it is difficult to distinguish in the presence of ice. In 2007 the fluctuations only become apparent in March, after the region has been ice-free for more than two months.

The temporal and spatial variability of the temperature fluctuations is best illustrated by means of power spectral analysis, which partitions variance as a function of frequency (Emery and Thomson, 2004). Fig. 5A shows power spectral density (PSD) for all temperature sensors during the ice-free season of deployment 2, when the fluctuations are observed most clearly. Several peaks are consistently present at different depths over this frequency range, and the decrease in variance with depth can be clearly observed. Hence, comparison between the different

deployments and between the two mooring sites (Fig. 5B and C) requires the selection of time series from similar depths. The instruments at 283, 274 and 273 m for the three RaTS deployments, respectively, and 298 m for MT are most appropriate for this. The spectra in Figs. 5B and C show several features of note: (1) variability in the 2–7 days band is consistently higher at the RaTS site than at MT; (2) RaTS deployment 2 shows the strongest variability; and (3) the difference in depths between the sensors is unlikely to be the most important factor in the observed differences between the spectra, as the sensors from RaTS deployments 2 and 3 are at virtually the same depth, yet show markedly different variability (i.e. the influence of time is strong compared with that of depth). Fig. 5D illustrates the difference between the RaTS and MT sites, where spectra for each site, along with their 95% confidence intervals, show that the RaTS site experiences stronger variability in the 2–7 days band than is observed at MT. This is unlikely to arise from differences in temperature gradients between the two sites, as they are virtually identical below 200 m during the summers of 2005–2007 (Fig. 2C). Finally, Fig. 5E illustrates the difference between the ice-free and ice-covered seasons for RaTS deployment 2, such that variability in the 2–7 days band is clearly higher in the absence of ice.

The 2–7 days fluctuations are most readily interpreted as oscillations of isotherms, and the broad frequency range of the oscillations indicates that they are forced by a strongly variable mechanism operating on a timescale of several days. The most obvious explanation for the observations is thus an oceanic

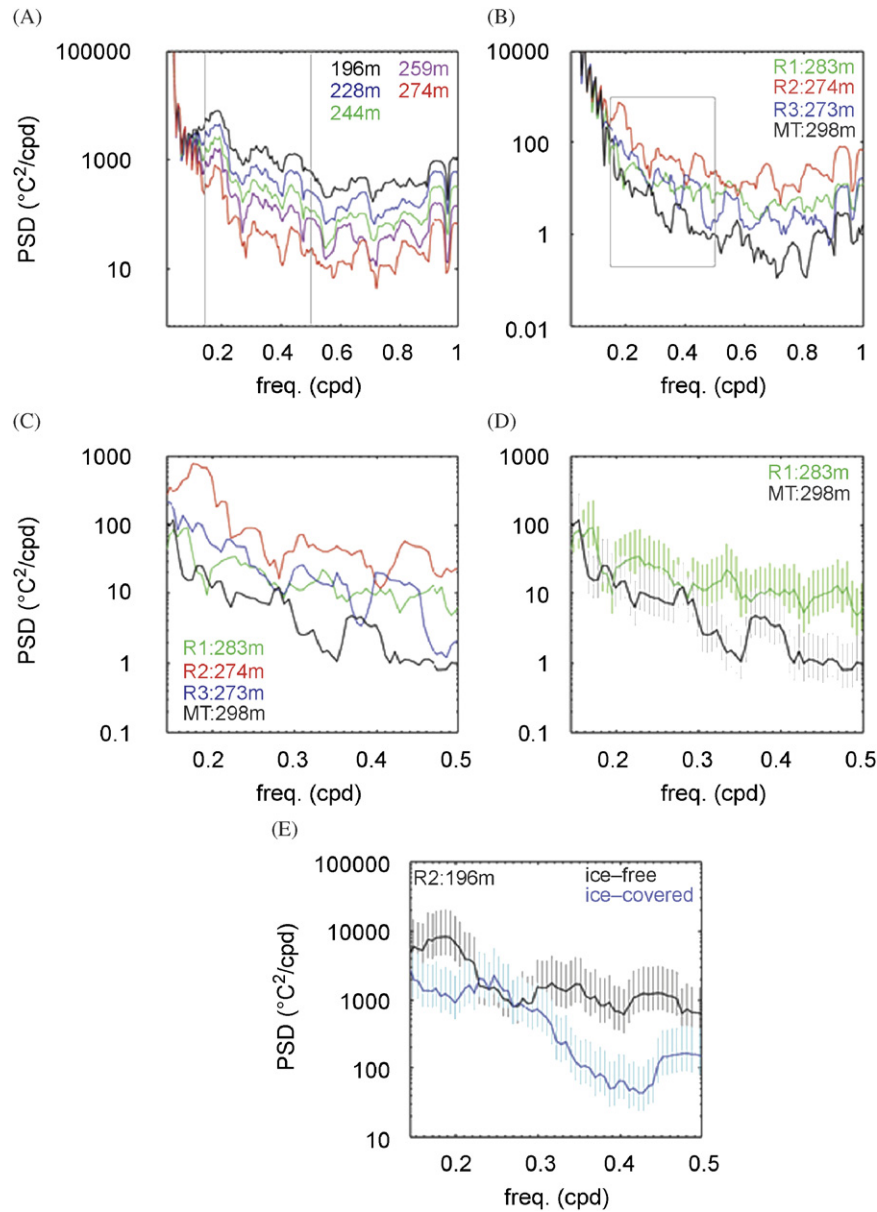


Fig. 5. Log-linear plots of power spectral density (PSD) for 126-day temperature time series: (A) for all sensors from RaTS deployment 2 during the ice-free season; (B) 298 m at MT, and 283, 274 and 273 m for RaTS deployments 1–3, respectively, for the ice-free season. The grey square marks the 2–7 days period, which is expanded in (C) for the four time series; (D) spectra from the MT mooring (black, 298 m) and RaTS deployment 1 (green, 283 m). Vertical lines represent the 95% confidence level; (E) spectra for the ice-free (black) and ice-covered (blue) seasons for RaTS deployment 2 (196 m).

response to wind forcing. Supporting this concept, temperature anomaly time series over the ice-free season correlate significantly with wind anomalies measured at Rothera, which are known to differ from those elsewhere on the WAP because of local topography (Beardsley et al., 2004). The oscillation is sensitive to wind direction, with the strongest correlation associated with northwest to southeastward winds. Correlations are positive with northwestward winds and negative with southeastward winds, indicating that the former lead to warming and the latter to cooling. Examples of the correlations are shown in Fig. 6 for the shallowest (CTD10822 at 202 m) and deepest (CTD10824 at 286 m) temperature sensors at the RaTS site for the 30-day period 26th January–24th February 2005. The intervening three temperature sensors show similar correlations. Winds lead the temperature signal by 27–36 h, and the correlations decrease with depth in the water column, from 0.56 at 202 m

to 0.36 at 286 m. All correlations are significant at either the 95% or 99% level (statistical significance is calculated following the method of Trenberth, 1984). No significant correlations are observed during the ice-covered season, which is consistent with the observed decrease in the magnitude of the oscillation, indicating a seasonal cycle in the winds and/or the ocean's response to the atmospheric forcing. Spectral analysis of NW–SE winds from the ice-free season shows significant peaks over the 2–7 days period that correspond with those observed in temperature time series, as shown in Fig. 7 for deployment 2.

The significant lagged correlations with the winds are consistent with wind-driven upwelling and downwelling behaviour, whereby a northwestward wind (i.e. parallel to the coast; Fig. 1B) tends to induce upwelling along the NE coast of Ryder Bay, leading to the observed temperature increase at depth, whilst a

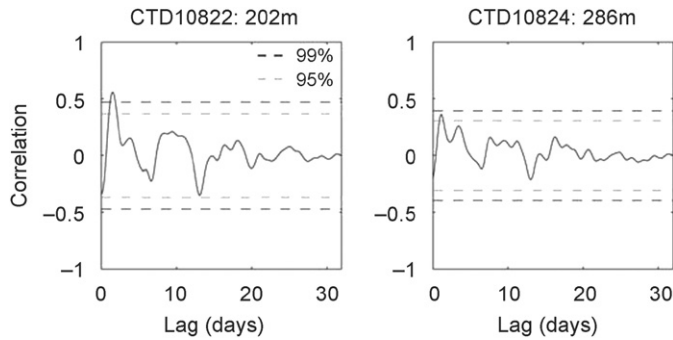


Fig. 6. Correlations of temperature and NW–SE wind anomalies for the 30-day period 26/1/05–24/2/05 during the ice-free season of RaTS deployment 1. Both the wind and oceanographic data are filtered using a 26-h Butterworth lowpass filter prior to correlation. The black and grey dashed lines represent the 95% and 99% significance levels, respectively.

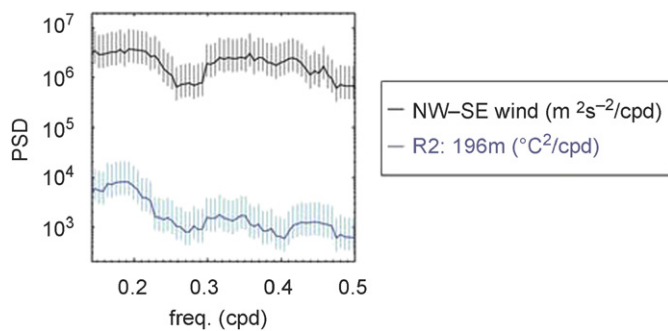


Fig. 7. Log-linear plots of power spectral density (PSD) for the NW–SE wind (black) and temperature at 196 m from RaTS deployment 2 during the ice-free season of 2006. Vertical lines represent the 95% confidence intervals for the wind (grey) and temperature (cyan) time series.

southeastward wind is associated with downwelling and a temperature decrease at depth. However, this simple correlation does not consider the cumulative response of the ocean to upwelling/downwelling favourable winds. For instance, [Austin and Barth \(2002\)](#) found that an index of coastal upwelling/downwelling in the ocean off the coast of Oregon was a function of the weighted cumulative alongshore wind stress on a timescale of 2–8 days. Following their method, we examine the coastal upwelling response (i.e. the observed temperature fluctuations) to the cumulative NW–SE wind stress (W , positive NW-ward), weighted to the most recent observations, over the cumulative upwelling timescale (t_c), according to the equation:

$$W \propto \int_{t^0/40}^{t_c} t^s e^{-\alpha(t-t_c)} dt \quad (2)$$

where t^s is the NW–SE wind stress and t^0 is time. The analysis is carried out over three 30-day periods for the ice-free and ice-covered season of each deployment ([Table 3](#)). As previously, wind and oceanographic time series are filtered using a 26-h Butterworth lowpass filter prior to analysis. Correlation of temperature time series with W for a number of different values of t_c reveal that upwelling/downwelling behaviour at the RaTS site responds to the cumulative NW–SE wind stress over a timescale of 17–90 h. These results are in conceptual agreement with those of [Austin and Barth \(2002\)](#). Fewer significant correlations are observed during the ice-covered season, and possible explanations for this include: (1) seasonal changes in stratification, leading to a change in the ocean's response to wind forcing; (2) a seasonal cycle in the wind forcing; and (3) damping of the ocean's response to the

Table 3

Time periods over which correlations were carried out between winds at Rothera and moored temperature time series

Deployment	Season	Dates
1	Ice-free	26/01/05–24/02/05
		27/02/05–28/03/05
1	Ice-covered	03/04/05–02/05/05
		03/06/05–02/07/05
		06/07/05–04/08/05
2	Ice-free	15/09/05–14/10/05
		18/02/06–19/03/06
2	Ice-covered	28/03/06–26/04/06
		30/04/06–29/05/06
		30/07/06–28/08/06
3	Ice-free	31/08/06–29/09/06
		30/09/06–29/10/06
		31/12/06–29/01/07
		30/01/07–28/02/07
		02/03/07–31/03/07

atmosphere by the presence of sea ice. Each of these possibilities is discussed in turn.

- (1) [Fig. 2](#) shows that buoyancy frequency is relatively stable below 200 m throughout the year, with only a small reduction in N during winter. This pattern is observed every year, and N is similar at these depths throughout the three deployments, yet the fluctuation clearly varies on both seasonal and interannual timescales. [Fig. 8](#) shows time series of monthly mean NW–SE wind stress anomaly, buoyancy frequency anomaly at each of the sensor depths (derived from the RaTS CTD profile data set) and t_c for significant correlations between each temperature sensor and the cumulative NW–SE wind stress. Significant correlations with cumulative wind stress are observed at all depths in the presence of both high and low N , so although we can expect the observed temporal variability of the fluctuations to be influenced by changes in stratification, the observations cannot be solely attributed to this cause.
- (2) The time series of wind-stress anomaly in [Fig. 8](#) shows that winds are generally stronger during the ice-covered season, which does not explain the observed temporal variability in the temperature fluctuations. Furthermore, significant correlations occur between temperature and NW–SE wind stress both when winds are anomalously strong and when they are anomalously weak, so the observations cannot be explained in terms of wind stress variability alone.
- (3) Periods of sea-ice cover are marked in [Fig. 8](#). In the presence of ice, the number of significant correlations is reduced, implying that the sea ice has a significant effect upon the transmission of wind stress to the deep ocean. This concept is supported by the rapidity of the response of the fluctuations to the presence of sea ice. Observations from Rothera Station suggest that sea-ice cover was more fragmented in Ryder Bay in 2006 than 2005, which is consistent with the relative strengths of the fluctuations during the two winters. Whether the decrease in the fluctuations during the ice-covered season is a response to local sea-ice conditions in Ryder Bay or those throughout the wider Marguerite Bay area cannot be determined without comprehensive, high-resolution sea-ice data across the region. Ryder Bay can be covered with fast ice whilst the ice in the rest of northern Marguerite Bay is fragmented, or vice versa, but several years' worth of data from both locations would be needed, along with comprehensive sea-ice observations, to unravel such connections.

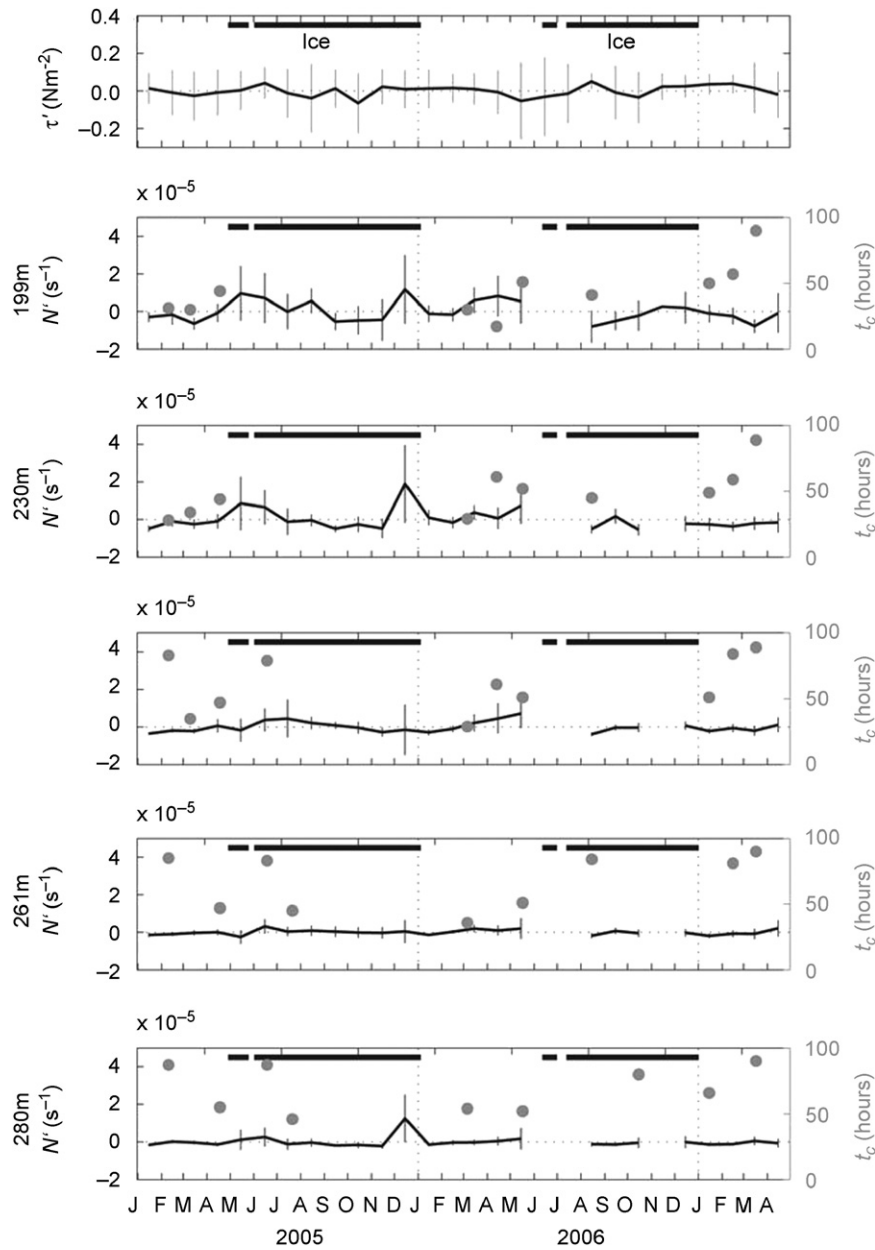


Fig. 8. Time series of monthly mean NW–SE wind stress anomaly (τ') at Rothera station and monthly mean buoyancy frequency anomalies (N') from the RaTS CTD profiles for depths corresponding to those of the five temperature sensors on the RaTS mooring (missing data are due to gaps in the CTD sampling program). Vertical lines indicate 7 ± 1 standard deviation. The mean depth of each sensor over the three deployments is noted to the left of each plot. The timescales (t_c) at which temperature perturbations best correlate with cumulative wind stress are marked by the grey dots (only those correlations significant at the 95% or 99% level are included). The thick black lines indicate periods of sea-ice cover.

The internal Rossby radius of deformation (r) sets the offshore length scale over which the influence of coastal upwelling is discernible. This can be estimated for the RaTS site via (from Emery and Thomson, 2004):

$$r \approx \frac{NH}{f\beta} \quad (3)$$

where a water depth of $H \approx 520\text{m}$ and a buoyancy frequency of $N \approx 2.1 \times 10^{-4}\text{s}^{-1}$ (which is the maximum value observed within UCDW) yields $r \approx 8\text{km}$. The RaTS site lies $\approx 2\text{km}$ from the NE coast of Ryder Bay, and is, therefore, well within one internal Rossby radius of the coast, whereas the MT mooring lies $\approx 15\text{km}$, more than an internal Rossby radius, from the nearest coastline.

When an upwelled density structure intersects the surface as an upwelling front, this front can be driven arbitrarily far offshore by sustained winds (Allen et al., 1995; Austin and Lentz, 2002), so the scale of upwelling influence is no longer set by the internal Rossby radius. In the present case, it is presumed that upwelling influence does remain within an internal Rossby radius of the coast for a number of reasons: we consider temperature levels that are in excess of 115 m deep at the mooring sites, winds that are highly variable, and an upwelling response that is expected to vary greatly depending on the local orientation of the coastline. In this setting, it seems unlikely that upwelling would be sufficiently sustained to bring these isotherms to the surface nearshore.

The lack of a clear upwelling signal at MT may be explained in two ways: (1) the upwelling influence is trapped within an

internal Rossby radius of the coastline, and so does not extend to MT; (2) winds at Rothera are known to differ from those in other areas of Marguerite Bay (Beardsley et al., 2004), so the correlation of temperature records from the RaTS site with Rothera winds may suggest that this upwelling behaviour is a relatively local phenomenon, which cannot therefore be expected to influence localities such as MT. Further investigation of this spatial variability would require data from several locations around Marguerite Bay.

The temporal variability of the quasi-periodic fluctuations is best investigated by comparison of the total variance, S^2 , over the 2–7 days period for each temperature sensor (Fig. 9). S^2 of 114-day time series, limited by the length of deployment 3, is shown for the ice-free and ice-covered seasons of each RaTS deployment, and values for the two seasons from the different deployments are compared in Table 4. In the shallowest two instruments, S^2 is 3–4 times as large during the ice-free season as in the presence of ice for both deployments 1 and 2. The difference in S^2 between the ice-free and ice-covered seasons becomes less pronounced in the deeper instruments during deployment 1, but remains at a factor of 3–4 during deployment 2 at all depths. Values from the ice-free season of deployment 2 are 2–8 times larger than those of deployments 1 and 3, whilst during the ice-covered season, values of S^2 from deployment 2 are 2–3 times larger than those from deployment 1.

Coastal upwelling involves both vertical and horizontal motion of the water column, thus the fluctuations observed at the RaTS site can be expected to arise from both vertical and lateral temperature gradients. Whilst our data from just two locations are not sufficient to fully determine the relative importance of

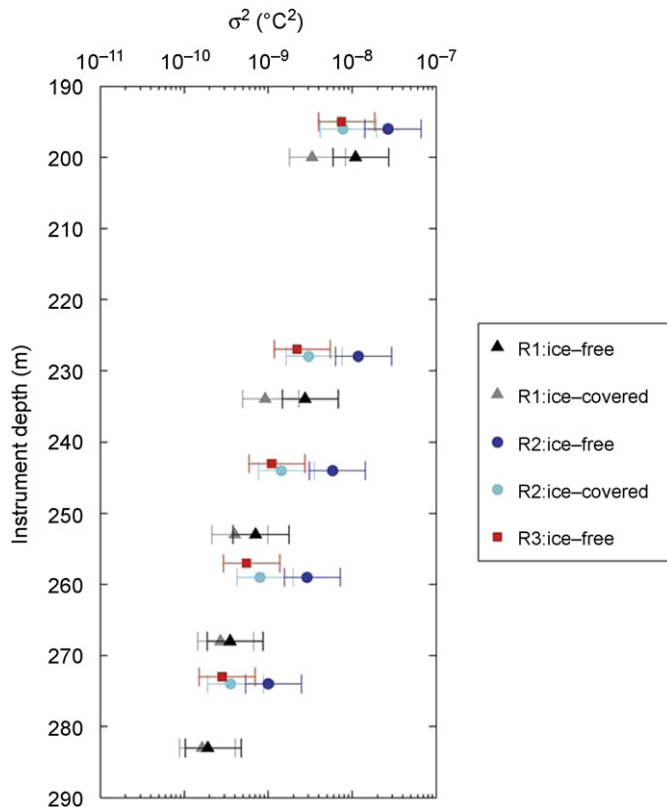


Fig. 9. Log-linear plot of variance (S^2) of temperature time series against instrument depth over the 2–7 days period for the ice-free and ice-covered seasons of the three RaTS deployments. Deployment 1 is represented by triangles (black and grey for the ice-free and ice-covered seasons, respectively); deployment 2 by circles (dark and light blue); and deployment 3 by red squares. Bars represent 95% confidence intervals.

Table 4

Comparison of variance over the 2–7 day period from the ice-free and ice-covered seasons for all instruments from the three RaTS deployments

Deployment	Depth (m)	$\frac{S_{no\ ice}^2}{S_{ice}^2}$	$\frac{S_{no\ ice}^2}{S_{no\ ice}^2 \cdot \frac{1}{3}}$	$\frac{S_{ice}^2}{S_{ice}^2 \cdot \frac{1}{3}}$
1	200	3.29	2.41	2.33
	234	2.97	4.31	3.29
	253	1.78	8.16	3.58
	268	1.30	8.28	2.94
	283	1.17	5.23	2.17
2	196	3.40		
	288	3.89		
	244	4.06		
	259	3.65		
	274	2.83		
3	195		3.56	
	227		5.38	
	243		5.26	
	257		5.27	
	273		3.56	

Comparisons include variance during the ice-free season divided by variance during the ice-covered season; variance during the ice-free season of deployment 2 divided by the corresponding data from the other two deployments; and variance from the ice-covered season of deployment 2 divided by that from the ice-covered season of deployment 1.

horizontal and vertical water motions in generating the temperature fluctuations, it is possible to estimate the magnitude of the vertical perturbations of the water column that would be required to generate the observed fluctuations, thereby providing a realistic upper limit for the amplitude of the coastal upwelling response. The depth perturbation, D^0 , is calculated from the representative temperature gradient, qT_{CTD}/qz , at depth z , and the magnitude of the temperature fluctuation, T_m^0 , measured at the mooring:

$$D^0 \approx \frac{T_m^0}{qT_{CTD}/qz} \tag{4}$$

such that a typical temperature perturbation of 0.3 °C at 200 m (during the ice-free season), with an average temperature gradient of 0.011 °C/m over the depth range 195–205 m, yields $D^0 \approx 27$ m. Deeper sensors experience smaller temperature perturbations, but the associated temperature gradients are also smaller, so values of D^0 are comparable between the different depths.

In summary, the quasi-periodic fluctuations observed at the RaTS site are a manifestation of coastal upwelling (downwelling) leading to a temperature increase (decrease) within the modified UCDW below 200 m depth. These oscillations are primarily driven by NW–SE-ward winds that induce upwelling/downwelling along the NE coast of Ryder Bay, 2 km from the RaTS site. The ocean’s response to the wind forcing has the potential to generate vertical perturbations of the water column of the order of several metres to a few tens of metres, and is damped in the presence of pack ice.

4.2. Internal tides

4.2.1. Quantification of the barotropic tide

When considering internal tides using subsurface measurements, it is important to be able to distinguish, and quantify the influence of, the barotropic tide. Here we use the AntPen04.01 tidal model (L. Padman, unpublished; www.esr.org/ptm_index) to estimate barotropic tides at both moorings locations. The tides in this region are relatively small, with velocities of $p\ 3.24\ cm\ s^{-1}$ at the RaTS site and $p\ 0.59\ cm\ s^{-1}$ at MT for the dominant diurnal (O1, K1) and semidiurnal (M2, S2) constituents (see Table 5).

Table 5
Amplitude and phase of the eastward (u) and northward (v) components of the dominant diurnal and semidiurnal tides for the two mooring sites

Tidal con.	Freq. (cpd)	RaTS site		MT site	
		u amp. (cm s^{-1}) [phase (deg)]	v amp. (cm s^{-1}) [phase (deg)]	u amp. (cm s^{-1}) [phase (deg)]	v amp. (cm s^{-1}) [phase (deg)]
M2	1.9323	1.05 [40.32]	3.24 [186.88]	0.37 [179.53]	0.17 [321.23]
S2	2.0000	1.68 [141.95]	2.54 [254.65]	0.59 [320.86]	0.57 [193.59]
K1	1.0027	0.83 [169.57]	0.39 [294.51]	0.39 [335.22]	0.36 [211.57]
O1	0.9295	0.78 [149.15]	0.97 [273.21]	0.34 [324.49]	0.23 [205.07]

Data are from the AntPen04.01 tidal model (Padman, unpublished; www.esr.org/ptm_index).

At the RaTS site, the velocities of the semidiurnal tides are roughly twice those of the diurnal tides. The M2 and S2 semidiurnal tides, and the O1 diurnal tide, are dominated by the northward component of flow, whilst the K1 diurnal tide is dominated by the eastward component of flow. In contrast, the tidal energy is more evenly distributed between the diurnal and semidiurnal constituents at MT, and all constituents detailed here are dominated by the eastward component of flow, although this dominance is weaker in the S2 and K1 tides.

As can be seen in Fig. 1, the RaTS site is located in an elongated basin oriented roughly E–W, whilst the MT site lies in a trough running NE–SW. Thus, the tidal energy available for the generation of baroclinic tides is likely to differ between the two sites, not only due to differences in the barotropic forcing, but also due to the respective orientations of the barotropic tides relative to the seabed topography.

4.2.2. Internal tides in the moored velocity records

Spectra of velocity data using 112-day time series from the moored upward-looking ADCPs at both mooring sites clearly show energy at tidal frequencies (Fig. 10). Spectra from the RaTS site show relatively strong diurnal tides in eastward velocity (u), whilst the semidiurnal tides are virtually absent, despite the stronger semidiurnal barotropic forcing detailed in Table 5. All tidal signals in northward velocity (v) are weak, despite stronger barotropic forcing in v than u for the M2, S2 and O1 constituents. Both seasonal and interannual variability are observed, with stronger tidal signatures during the ice-free season, and lower tidally induced variance during deployment 3 compared with the other deployments. During the ice-free season, distinct changes in the strength of the diurnal tidal peaks are observed with depth, with PSD(u) from all three deployments showing a distinctive pattern of relatively high PSD close to the surface and below 90 m, and a band of low values centred at 50 m. This is highlighted in Fig. 11, which shows spectra and confidence intervals for u and v at selected depths.

At MT, the energy at diurnal frequencies is comparable to that at the RaTS site, whilst that at semidiurnal frequencies is significantly higher, despite the diurnal barotropic forcing being comparable to the M2 semidiurnal forcing. The energy at the semidiurnal frequencies is likely subject to contributions from the observed strong, near-inertial energy (f is very close to the frequencies of the semidiurnal tides at this latitude). However, non-tidal near-inertial currents would be expected to generate a broad peak in PSD, whereas the M2 and S2 peaks are well defined, indicating that the semidiurnal tidal energy is indeed strong compared with the diurnal energy. The diurnal tides also show slightly higher flow in v than u , despite marginally stronger barotropic forcing in the eastward component of flow. The energy associated with the O1, K1 and M2 tidal frequencies changes with depth, particularly during the ice-free season, where they decrease to roughly zero between 50 and 100 m, but there is no

increase in energy at depth analogous to that observed at the RaTS site. Selected spectra (and confidence intervals) from MT are also shown in Fig. 11.

To summarise, velocity data recorded at the two mooring sites show tidal signals that differ from both their respective barotropic forcings and from each other, and the strength of the tidal signals changes with depth at both mooring sites. The particularly strong semidiurnal energy at MT is likely to be influenced by near-inertial currents of non-tidal origin, with particularly strong semidiurnal tidal currents also present. During the ice-free period, other frequencies (from 0.5 to 2.0 cpd) also show surface-intensified energies at MT, and their absence during the ice-covered periods is strongly suggestive of atmospheric processes being responsible. (This range of frequencies includes the diurnal tidal band, explaining the surface-intensification of diurnal tidal energy during the ice-free months at MT.) In contrast, the RaTS site does not experience significant near-inertial energy, and whilst there is evidence of higher energies in the near-surface layers during the ice-free months, the observed depth-dependence of the diurnal tidal energy cannot be explained solely by atmospheric forcing covering a range of frequencies that includes the diurnal band. In particular, the energy at diurnal frequencies does not consistently decrease away from the surface, but instead shows a relative minimum in energy at around 50 m. This is consistent with the presence of internal (baroclinic) tides at the RaTS site.

The tidal currents show distinct interannual variability and are generally reduced during the ice-covered season, which can be attributed in part to temporal changes in stratification (Fig. 2). However, both seasonal and interannual changes in N are of the same order of magnitude (10^{-3} s^{-1}), yet seasonal variability in PSD is clearly far stronger than interannual variability, so the observed changes cannot be attributed to variability in N alone. Given that the barotropic forcing is not expected to show strong temporal variability, the decrease in tidal currents in the presence of ice indicates the existence of a potentially important relationship between tides and sea ice, which is worthy of further investigation. Another likely influence upon baroclinic tidal flow is low frequency current variability (Wallace, 2007), which, by altering the background density field and introducing background shears, can influence the pathways along which internal wave energy travels, and thus the manner in which it interacts with bathymetry (Sherwin and Taylor, 1990).

To confirm the presence of internal tides we conducted harmonic analysis of ADCP current data using the Matlab package T_TIDE (Pawlowicz et al., 2002). Fig. 12 shows profiles of tidal phase extracted for the O1, K1, M2 and S2 tides at the RaTS site and MT. Phase shifts of 180°, characteristic of internal tides (Gill, 1982), are observed at the RaTS site, whilst no such phase shifts occur at MT. However, it is necessary to consider that the MT ADCP samples the upper 100 m of a water column that is 4800 m deep, so the lack of phase change measured at this

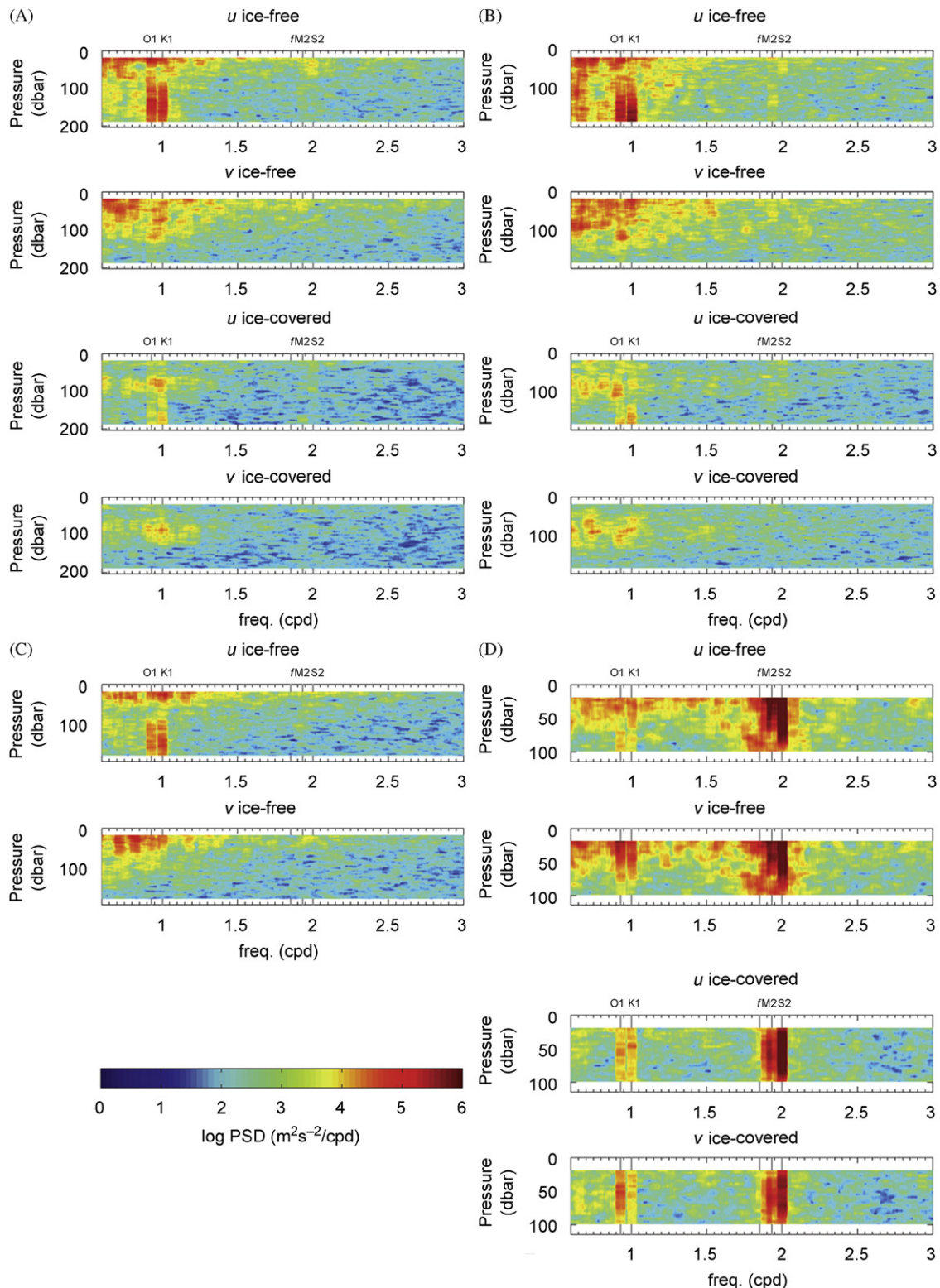


Fig. 10. Contour plots of power spectral density (PSD) for east (u) and north (v) velocities from the moored ADCPs at (A–C) the RaTS site for all deployments and (D) MT. Spectra for both the ice-free and ice-covered seasons are included, where available. The O1, K2, M2, S2 and inertial (F) periods are marked. Note the different depth scales at the two mooring sites. Frequency measured in cycles per day.

location does not necessarily indicate the absence of internal tides. The RaTS data show a larger number of 1801 phase changes for the semidiurnal than the diurnal constituents, but due to the low tidal energy at the semidiurnal frequencies at this site, and the associated difficulties of relating phase information to the

observed variability, the following discussion will concentrate upon the diurnal tides during the ice-free season, and in particular the eastward component of flow.

The phase profiles at the RaTS site highlight three primary regimes of variability over the depth profiles: (1) relatively

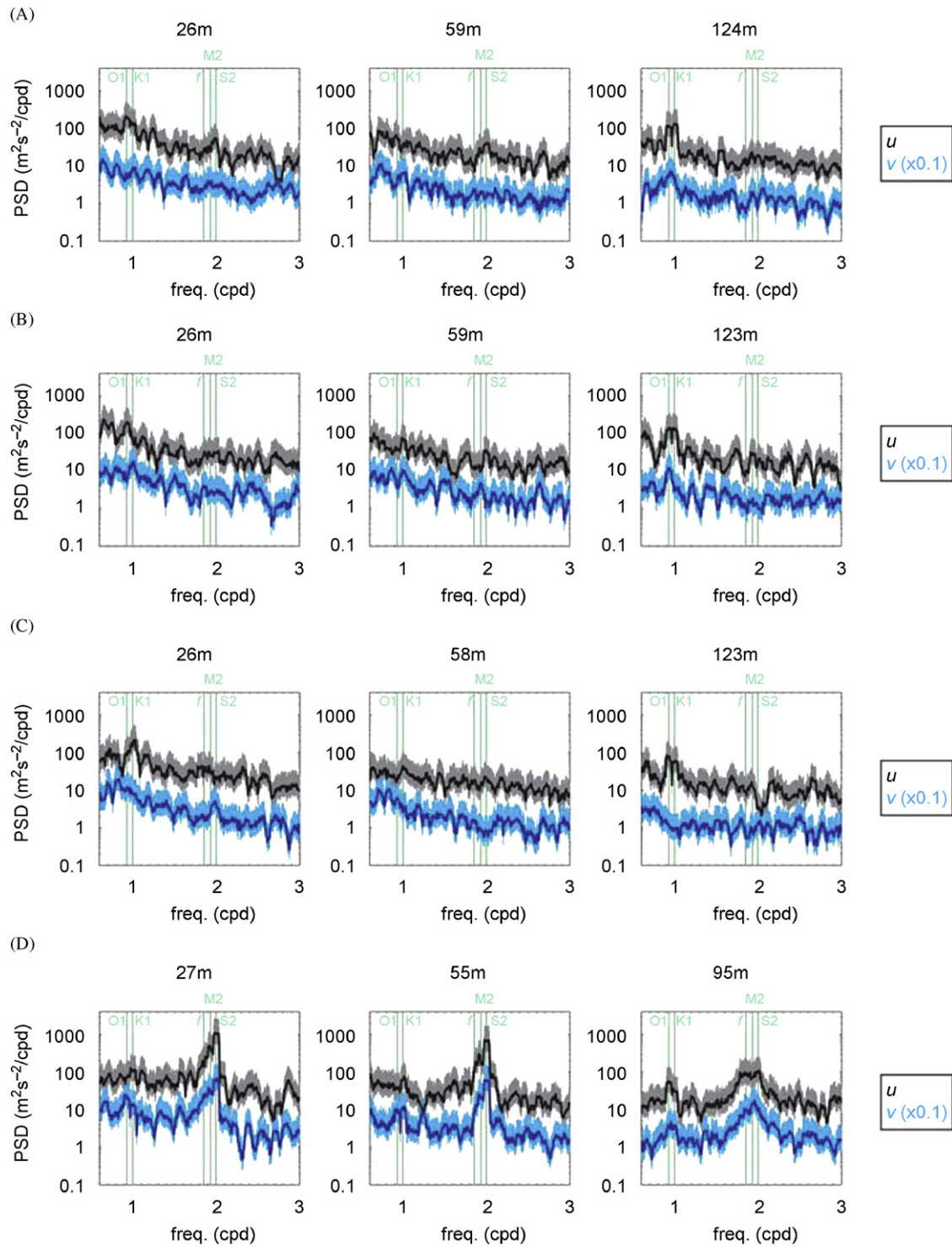


Fig. 11. Confidence levels for ADCP velocity PSD for selected depths from (A to C) the three RaTS deployments and (D) MT. Eastward velocity (u) and northward velocity (v) are shown in black and dark blue, with their respective 95% confidence levels in grey and light blue. PSD(v) is multiplied by 0.1 for ease of viewing. Frequencies of the O1, K1, M2 and S2 semi-diurnal tides are marked in light green, as is the inertial frequency, f .

high variability above 40m, characterised by 1801 phase shifts in O1 and K1 of deployment 2, and O1 of deployment 3; (2) low variability between 40 and 100–120m, characterised by virtually constant phase; and (3) high variability below 100–120m, characterised by between one and ten 1801 phase changes. These phase changes indicate regions of high shear and correspond well with the near-surface and deep regions of high energy shown in u in Fig. 10, and/or the transi-

tions between regions of high and low energy, whilst the relatively stable phase profile between 40 and 100–120m corresponds well with the low energy observed at these depths. However, the relatively constant phase throughout the shallow water column for O1 and K1 of deployment 1, and K1 of deployment 3, indicates that relatively large changes in PSD with depth need not be associated with current reversals.

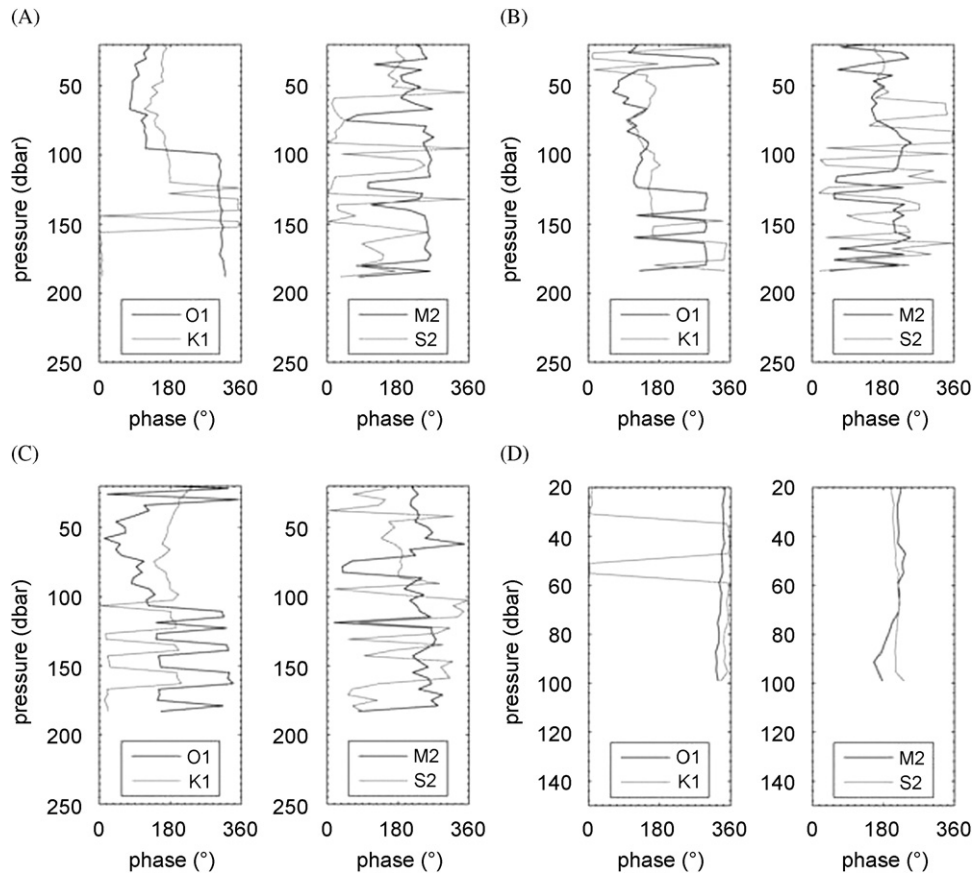


Fig. 12. Profiles of tidal phase for the diurnal O1 and K1, and semidiurnal M2 and S2 tides for the three RaTS deployments and MT. Profiles are extracted from the ADCP data using the harmonic analysis package, T_TIDE (Pawlowicz et al., 2002).

Profiles of diurnal tidal amplitude are also in good agreement with the results from the RaTS PSD analysis (Fig. 13A–C), with the lowest amplitudes observed where PSD is lowest. This change in tidal amplitude with depth is also indicative of baroclinic tides (a barotropic tide should not show such variability), confirming their importance at the RaTS site. Amplitude profiles from MT (Fig. 13D) also show a decrease with depth, particularly at the semidiurnal frequencies, which is again consistent with the observed patterns in PSD. This indicates that, even though no phase change is observed at this location, the site is influenced by internal tides.

4.2.3. Generations sites of internal tides

The inconsistencies between the expected and observed relative strengths of the eastward and northward components of tidal flow at the RaTS site suggest that the orientation of the flow with respect to seabed topography is important. The location of Marguerite Bay poleward of the critical latitude for diurnal internal tides, but equatorward of that for semidiurnal internal tides, implies that the superinertial semidiurnal signal should be allowed to propagate freely (although it may be locally generated), whilst we expect the subinertial diurnal internal tide to be generated in the region of our moorings or to have propagated along the coastline or local bathymetric slope with an offshore or off-slope horizontal length scale of the order of the internal Rossby radius. The strong diurnal internal signal at the RaTS site is thus consistent with its proximity to the coast.

Internal tides have been observed in the Arctic (Konyaev et al., 2000; Morozov et al., 2003) and around the margins of Antarctica

(Foldvik et al., 1990; Levine et al., 1997; Albrecht et al., 2006), and both models (Morozov and Pisarev, 2002; Padman et al., 2006) and observational work (Albrecht et al., 2006) suggest that the interaction of barotropic flows with seabed topography is an important process in the generation and propagation of internal tides. In order to identify potential generation sites in the vicinity of the two mooring sites we derive the internal tidal forcing function, F , after Sherwin (1988):

$$F = \frac{izQN^2}{\omega} \mathbf{r} \cdot \frac{1}{H} \quad (5)$$

where Q is the tidal flow (defined as uH, vH , where u and v are the eastward and northward velocities, and H the water depth), ω is the frequency of the internal tide, z is the depth of interest, and $\mathbf{r} = \nabla \left(\frac{1}{H} \right)$ is the horizontal gradient of the inverse of the water depth. Bathymetry data are from the US SO-GLOBEC program (www.whoi.edu/science/PO/so_globec/WHOI_tech_report) and are used internally in AntPen04.01 to calculate uH and vH across the regions around each mooring site marked in Fig. 1. The calculation is carried out for both the ice-free and ice-covered seasons of all years at the RaTS site, but results are shown here for 2006 only. Deployments 1 and 3 show results consistent with those presented here. Average profiles of N are calculated for the ice-free and ice-covered seasons from CTD profiles collected from February to June 2006 and July to November 2006, respectively. The analysis is carried out for both the K1 and M2 internal tides, in order to permit comparison of the potential local generation sites for both diurnal and semidiurnal internal tides. F is also calculated for the K1 and M2 tides during the ice-free season

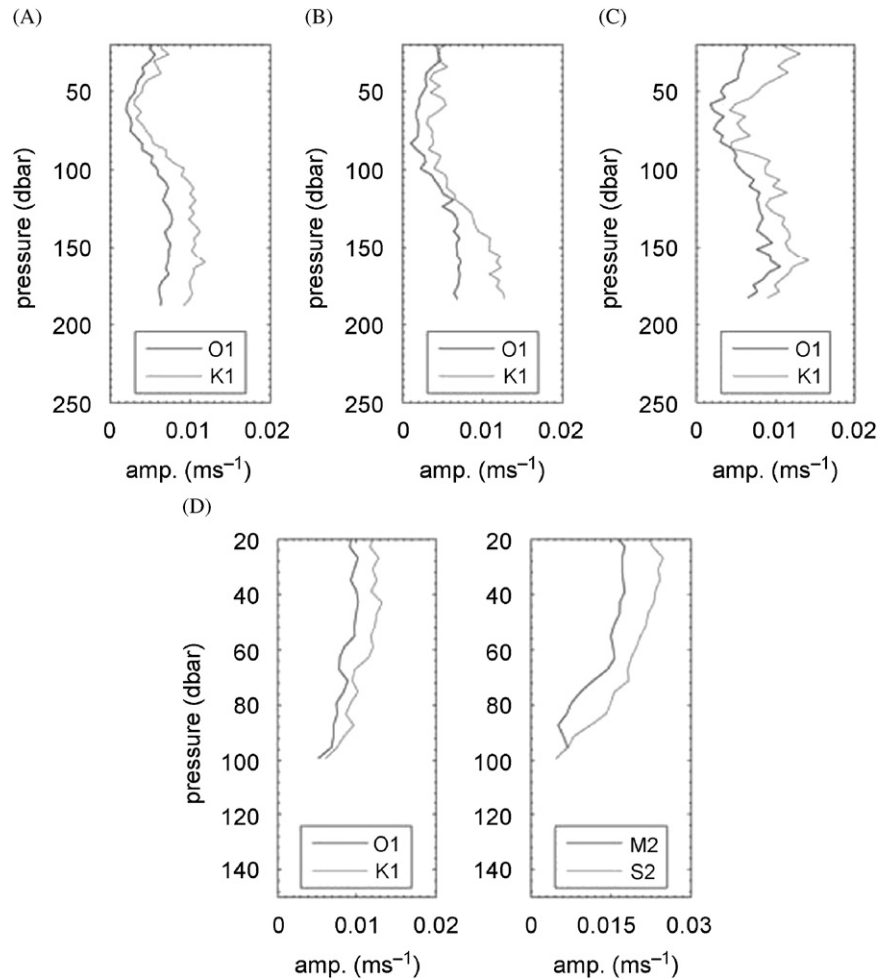


Fig. 13. Profiles of tidal amplitude for the diurnal O1 and K1 tides for the (A–C) three RaTS deployments and (D) MT, and the semidiurnal M2 and S2 for MT. Profiles are extracted from the ADCP data using the harmonic analysis package, T_TIDE (Pawlowicz et al., 2002).

at MT, using a profile of N derived from a CTD cast carried out at this location during February 2006. In the absence of winter CTD profiles at this location, F cannot be calculated for the ice-covered season.

Fig. 14A–D shows depth-integrated tidal forcing function, F^* , for the region around the RaTS site marked in Fig. 1. For both tidal constituents, values of F^* are of the order of $1\text{--}2\text{ N m}^{-2}$ over much of the domain but can be $4\text{--}50\text{ N m}^{-2}$ over areas of rugged bathymetry. At MT (Fig. 14E and F), F^* is generally higher, particularly for K1, with values of 10 N m^{-2} over much of the region and, again $4\text{--}50\text{ N m}^{-2}$ over areas of rugged bathymetry. These results echo those of Sherwin (1988) and Sherwin and Taylor (1990), who studied internal tides generated over the region of the Malin Shelf, north of Ireland. Sherwin and Taylor (1990) derived the highest values of F^* ($\approx 60\text{ N m}^{-2}$) at the continental shelf break and values of $10\text{--}20\text{ N m}^{-2}$ over the continental slope. The results of Sherwin (1988) were similar, with values of F^* $\approx 40\text{ N m}^{-2}$ at the shelf break and, again, $10\text{--}20\text{ N m}^{-2}$ over the continental slope, and he concluded that both regions were important for the generation of the observed internal tides.

The similarity of F^* derived for the Malin Shelf and Marguerite Bay is worthy of note, given that N measured on the Malin Shelf was roughly twice that in Marguerite Bay and the tidal forcing of the North Atlantic is an order of magnitude larger

than that on the WAP (Sherwin, 1988). We therefore conclude that the rugged nature of the WAP bathymetry, as reflected in $r\ \delta l = H\delta$ has the potential to induce relatively strong baroclinic tides, despite the weak barotropic forcing and weak stratification.

Potential generation sites for the diurnal internal tide observed at the RaTS site are the NE coastline and around the small islands to the SW side of Ryder Bay. Values of F^* are slightly higher over the region for the M2 internal tide due to larger values of Q (see details of tidal current flow in Table 5), although this is offset in part by the increase in O , and lower during the ice-covered season for both tidal constituents due to reduced stratification. However, given the similarities between the four maps, the influences of Q , N and O are clearly small compared to that of the bathymetry. Maps of F^* for the eastward and northward components of flow are not shown separately here, but vH accounts for 69% of the diurnal Q and 75% of the semidiurnal Q . Thus, the observed temporal variability in PSD, the differences between PSD of the diurnal and semidiurnal constituents, and the marked dominance of PSD(u) over PSD(v) cannot be solely attributed to differences in internal tide generation sites, or orientation of the tidal flow with respect to the known bathymetry.

At MT, most of the potential generation sites are located around the northern and western margins of the trough in which the mooring lies. The areas of high F^* ($4\text{--}20\text{ N m}^{-2}$) are

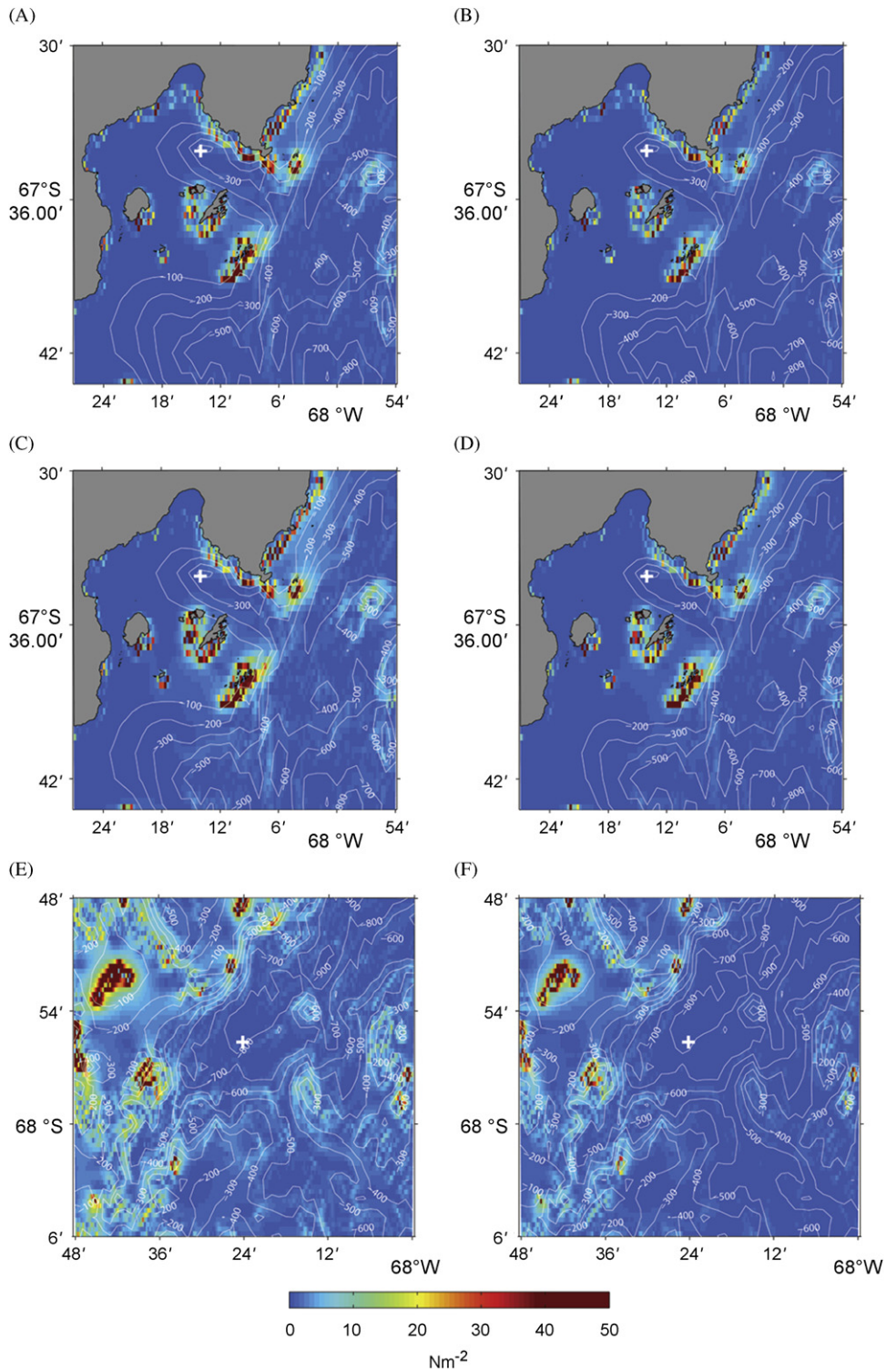


Fig. 14. Depth integrated tidal forcing function (F^*) calculated for (A, B) the K1 and (C, D) the M2 tides during the ice-free and ice-covered seasons of RaTS deployment 1, and (E, F) the K1 and M2 tides during the ice-free season at MT. The mooring locations are signified by white crosses and contoured depths are in metres (courtesy of the SO-GLOBEC program). The land is shaded grey and detailed coastline data for Ryder Bay are courtesy of MAGIC, BAS.

similar for both the diurnal and semidiurnal constituents, but the higher value of O for the semidiurnal tide leads to a clear decrease in F^* over much of the domain. In contrast to the RaTS site, uH dominates Q , accounting for 61% of the diurnal Q and 67% of the semidiurnal Q . Given that u and v are similar for K1, this shows that the orientation of the tidal flow with respect to the topography is an important factor.

5. Discussion

This study has shown that northern Marguerite Bay is affected by internal tides, although their nature differs between the nearshore RaTS site and the offshore MT site. At the RaTS site, energy at the diurnal frequencies dominates over the semidiurnal energy, despite stronger barotropic forcing at

semidiurnal frequencies. The orientation of the tidal flow with respect to seabed topography is also important, with higher energy observed in the eastward component of tidal flow for both the O1 and K1 internal tides, despite O1 being subject to stronger northward barotropic flow. An investigation of internal tide generation sites around Ryder Bay also indicates that the northward component of flow has more potential for generating internal tides, due to its orientation with respect to bathymetric features. However, observations show stronger tidal flow in the eastward direction, implying that the relationship between the forcing and propagation of the internal tides is complex. In addition, the RaTS site is influenced by quasi-periodic temperature fluctuations that we have shown are due to local wind-forced coastal upwelling and downwelling.

At MT, tidal energy is far stronger at the semidiurnal frequencies than the diurnal frequencies, despite similar barotropic forcing. Atmospherically forced signals are observed to contribute to the energy at both the diurnal and semidiurnal frequencies, but the signatures of the baroclinic tides can still be observed in the upper water column. Again, the orientation of tidal flow with respect to seabed topography is important, with the eastward component of flow having the strongest potential for internal tide generation.

There are a number of possible explanations for the temporal variability of both the atmospherically and tidally forced signals. The most likely are: (1) changes in stratification, whereby stronger stratification leads to a stronger internal wave signal due to higher variance at the depth of interest; (2) changes in background vertical shear arising from low frequency current variability; and (3) changes in sea-ice conditions, which appear to affect tidal flow and have the potential to influence the atmospherically forced signal, such that ice thickness, coherence and ridging can influence the transmission of wind-forcing to the ocean (e.g., Steele et al., 1989; Andreas et al., 1993; McPhee et al., 1999). Considering each of these possibilities in turn:

- (1) Changes in stratification undoubtedly influence the temporal variability of both the atmospherically forced and baroclinic tidal flows. However, it has been demonstrated that neither seasonal nor interannual changes in stratification can account for all of the variability in either the atmospherically forced signal or the internal tides.
- (2) Seasonal and interannual changes in low frequency currents have been observed in the uppermost 200 m of the water column at the RaTS site (Wallace, 2007) and are likely to account for some of the changes in internal tidal activity that are not related to stratification. There are, however, currently insufficient data for a full investigation of this theory.
- (3) The rapid response and decay of the atmospherically forced signal to the onset of pack ice clearly indicates that sea-ice conditions have an important influence upon the oscillations. Observations from Rothera Research Station suggest that the ice was more fragmented during the winter of 2006 than 2005, which is consistent with the continuation of the (albeit weakened) oscillation throughout the ice-covered season of 2006. More detailed ice data (including thickness, degree of ridging etc) are required to assess further the dynamical role of ice in suppressing atmospherically forced oscillations. The seasonal variability in the tidal energy at the RaTS site is likely linked to sea-ice conditions, but the nature of this connection is as yet unclear.

6. Conclusions

We conclude that internal perturbations in northern Marguerite Bay are subject to a number of influences, including local

winds, sea ice, barotropic tides and stratification. The observed internal wave and coastal upwelling activity may contribute to vertical mixing and nutrient distribution in Ryder Bay, with potential consequences for the operation of the local ecosystem; this is thus worthy of further investigation. The presence of a wind-driven signal beneath the permanent pycnocline at the RaTS site indicates that the UCDW is, locally at least, subject to some degree of atmospheric forcing, implying that changes in sea-ice cover or atmospheric circulation could have implications for mixing processes in these deep waters. The absence of the wind-driven signal at the MT site demonstrates that Ryder Bay is subject to at least some different forcing mechanisms to those of the more open waters of Marguerite Bay, as does the difference in the internal tidal signals between the two locations. The RaTS programme is continuing in Ryder Bay, and we are planning to redeploy our fixed moorings within the next few years, including deployments at other sites within Marguerite Bay and on the broader WAP shelf. This will allow us to quantify better the roles of the processes elucidated above, and to assess the local impacts of the internal waves and coastal upwelling on the marine ecosystem.

Acknowledgements

We thank personnel at the British Antarctic Survey's Rothera Research Station, particularly the Marine Assistants and boatmen, without whom the collection of RaTS CTDs since 1998 would not have been possible. Thanks also to the scientists and crew aboard the R.R.S. James Clark Ross and the RV Laurence M. Gould, and to the mooring technicians from the National Oceanography Centre, Southampton, for all their help and hard work. Many thanks to Bob Beardsley for providing the SO-GLOBEC data used here, the Proudman Oceanographic Laboratory for the Rothera tide gauge data and Laurie Padman for the AntPen04.01 model data. Thanks also to Carlos Moffat and an anonymous reviewer for positive and constructive feedback on this paper. The Rothera Time Series, Marguerite Bay moorings and Margaret Wallace's Ph.D. studentship were funded by the Natural Environment Research Council in the AFI Scheme, grant number NER/S/S/2004/13013.

References

- Albrecht, N., Vennell, R., Williams, M., Stevens, C., Langhorne, P., Leonard, G., Haskell, T., 2006. Observation of sub-inertial internal tides in McMurdo Sound, Antarctica. *Geophysical Research Letters* 33, L24606.
- Allen, J.S., Newberger, P.A., Federiuk, J., 1995. Upwelling circulation on the Oregon continental shelf. Part I: response to idealized forcing. *Journal of Physical Oceanography* 25, 1843–1866.
- Andreas, E.L., Lange, M.A., Ackley, S.F., Wadhams, P., 1993. Roughness of Weddell sea ice and estimates of the air-ice drag coefficient. *Journal of Geophysical Research* 98 (C7), 12439–12452.
- Austin, J.A., Barth, J.A., 2002. Variation in the position of the upwelling front on the Oregon shelf. *Journal of Geophysical Research* 107 (C11), 3180.
- Austin, J.A., Lentz, S.J., 2002. The inner shelf response to wind-driven upwelling and downwelling. *Journal of Physical Oceanography* 32, 2171–2193.
- Beardsley, R.C., Limeburner, R., Owens, W.B., 2004. Drifter measurements of surface currents near Marguerite Bay on the western Antarctic Peninsula shelf during austral summer and fall, 2001 and 2002. *Deep-Sea Research II* 51, 1947–1964.
- Clarke, A., Meredith, M.P., Wallace, M.I., Brandon, M.A., Thomas, D.N., 2008. Seasonal and interannual variability in temperature, chlorophyll and macronutrients in northern Marguerite Bay, Antarctica. *Deep-Sea Research II*, this issue [doi:10.1016/j.dsr2.2008.04.035].
- Costa, D.P., Crocker, D.E., 1996. Marine mammals of the Southern Ocean. In: Ross, R.M., Hofmann, E.E., Quetin, L.B. (Eds.), *Foundations for Ecological Research West of the Antarctic Peninsula*, Antarctic Research Series 70. AGU, Washington, DC, pp. 287–301.
- Dinniman, M.S., Klinck, J.M., 2004. A model study of circulation and cross-shelf exchange on the west Antarctic Peninsula continental shelf. *Deep-Sea Research II* 51, 2003–2022.
- Emery, W.J., Thomson, R.E., 2004. *Data Analysis Methods in Physical Oceanography*. Elsevier, Amsterdam.

- Foldvik, A., Middleton, J., Foster, T., 1990. The tides of the southern Weddell Sea. *Deep-Sea Research* 37, 1345–1362.
- Fraser, W.R., Trivelpiece, W.Z., 1996. Factors controlling the distribution of seabirds: winter–summer heterogeneity in the distribution of Adélie penguin populations. In: Ross, R.M., Hofmann, E.E., Quetin, L.B. (Eds.), *Foundations for Ecological Research West of the Antarctic Peninsula*, Antarctic Research Series 70. AGU, Washington, DC, pp. 257–272.
- Gill, A.E., 1982. *Atmosphere–Ocean Dynamics*. International Geophysics Series 30. Academic Press, San Diego, California.
- Gregg, M.C., 1987. Diapycnal mixing in the thermocline: a review. *Journal of Geophysical Research* 92 (C5), 5249–5286.
- Halpern, D., 1976. Structure of a coastal upwelling event observed off Oregon during July 1973. *Deep-Sea Research* 23, 495–508.
- Hofmann, E.E., Klinck, J.M., 1998. Thermohaline variability of the waters overlying the West Antarctic Peninsula Continental Shelf. In: Jacobs, S., Weiss, R. (Eds.), *Oceans, Ice and Atmosphere: Interactions at the Antarctic Continental Margin*, Antarctic Research Series 75. AGU, Washington, DC, pp. 67–81.
- Howard, S.L., Hyatt, J., Padman, L., 2004. Mixing in the pycnocline over the western Antarctic Peninsula shelf during Southern Ocean GLOBEC. *Deep-Sea Research II* 51, 1965–1979.
- Hyatt, J., Visbeck, M., Beardsley, R., Owens, W.B., 2008. Measurements of sea ice properties using a moored upward-looking acoustic Doppler current profiler (ADCP). *Deep-Sea Research II* 55, 351–364.
- Klinck, J.M., 1998. Heat and salt changes on the continental shelf west of the Antarctic peninsula between January 1993 and January 1994. *Journal of Geophysical Research* 103 (C4), 7617–7636.
- Klinck, J.M., Hofmann, E.E., Beardsley, R.C., Salihoglu, B., Howard, S., 2004. Water-mass properties and circulation on the west Antarctic Peninsula Continental Shelf in Austral Fall and Winter 2001. *Deep-Sea Research II* 51, 1925–1946.
- Koentopp, M., Eisen, O., Kottmeier, C., Padman, L., Lemke, P., 2005. Influence of tides on sea ice in the Weddell Sea: investigations with a high-resolution dynamic–thermodynamic sea ice model. *Journal of Geophysical Research* 110 (C02014), 137–158.
- Konyaev, K.V., 2000. Internal tide at the critical latitude. *Izvestiya, Atmospheric and Oceanic Physics* 36 (3), 363–375.
- Konyaev, K.V., Plueddemann, A., Sabinin, K.D., 2000. Internal tide on the Yermak Plateau in the Arctic Ocean. *Izvestiya, Atmospheric and Oceanic Physics* 36 (4), 542–552.
- Kowalik, Z., Proshutinsky, A.Y., 1994. The Arctic Ocean tides. In: Johansse, O.M., Muench, R.D., Overland, J.E. (Eds.), *The Polar Oceans and their role in shaping the Global Environment*, Geophysical Monograph 85. AGU, Washington, DC, pp. 137–158.
- LeBlond, P., Mysak, L.A., 1978. *Waves in the Ocean*. Elsevier Oceanographic Series 20. Elsevier, Amsterdam.
- Levine, M.D., Padman, L., Muench, R.D., Morison, J.H., 1997. Internal waves and tides in the western Weddell Sea: observations from Ice Station Weddell. *Journal of Geophysical Research* 102 (C1), 1073–1089.
- Mackinnon, J.A., Gregg, M.C., 2005. Spring mixing: turbulence and internal waves during restratification on the New England shelf. *Journal of Physical Oceanography* 35, 2425–2443.
- Martinson, D.G., Stammerjohn, S.E., Iannuzzi, R.A., Smith, R.C., Vernet, M., 2008. Palmer, Antarctica, Long-term Ecological Research Program first twelve years: physical oceanography, spatio-temporal variability. *Deep-Sea Research II*, this issue [doi:10.1016/j.dsr2.2008.04.038].
- McPhee, M.G., Kottmeier, C., Morison, J.H., 1999. Ocean heat flux in the central Weddell Sea during winter. *Journal of Physical Oceanography* 29, 1166–1179.
- Meredith, M.P., Renfrew, I.A., Clarke, A., King, J.C., Brandon, M.A., 2004. Impact of the 1997/98 ENSO on upper ocean characteristics in Marguerite Bay, western Antarctic Peninsula. *Journal of Geophysical Research* 109, 9013–9032.
- Mitchum, G.T., Clarke, A.J., 1986. The frictional nearshore response to forcing by synoptic scale winds. *Journal of Physical Oceanography* 16, 934–946.
- Morozov, E.G., Pisarev, S.V., 2002. Internal tides at the Arctic latitudes (numerical experiments). *Oceanology* 42 (2), 165–173.
- Morozov, E.G., Pisarev, S.V., Neiman, V.G., Erofeeva, S.Y., 2003. Internal tidal waves in the Barents Sea. *Doklady Earth Sciences* 393 (8), 686–688 (translated from Russian).
- Muench, R.D., Padman, L., Howard, S.L., Fahrback, E., 2002. Upper ocean diapycnal mixing in the northwestern Weddell Sea. *Deep-Sea Research II* 49, 4843–4861.
- Munk, W., Wunsch, C., 1998. Abyssal recipes II. *Deep-Sea Research I* 45, 1977–2010.
- New, A.L., 1988. Internal tidal mixing in the Bay of Biscay. *Deep-Sea Research* 35 (5), 691–709.
- New, A.L., Pingree, R.D., 1990. Evidence for internal tidal mixing near the shelf break in the Bay of Biscay. *Deep-Sea Research* 37 (12), 1783–1803.
- Ostrovsky, I., Yacobi, Y.Z., Walline, P., Kalikhman, I., 1996. Seiche-induced mixing: its impact on lake productivity. *Limnology and Oceanography* 41 (2), 323–332.
- Padman, L., Fricker, H.A., Coleman, R., Howard, S., Erofeeva, L., 2002. A new tide model for the Antarctic ice shelves and seas. *Annals of Glaciology* 34, 247–254.
- Padman, L., Howard, S., Muench, R., 2006. Internal tide generation along the South Scotia Ridge. *Deep-Sea Research II* 53, 157–171.
- Pawlowicz, R., Beardsley, B., Lentz, S., 2002. Classical tidal harmonic analysis including error estimates in MATLAB using T_TIDE. *Computers and Geoscience* 28, 929–937.
- Polzin, K.L., Toole, J.M., Ledwell, J.R., Schmitt, R.W., 1997. Spatial variability of turbulent mixing in the abyssal ocean. *Science* 276, 93–96.
- Pond, S., Pickard, G.L., 1983. *Introductory Dynamical Oceanography*, second ed. Pergamon Press, Oxford.
- Rippeth, T.P., Inall, M.E., 2002. Observations of the internal tide and associated mixing across the Malin Shelf. *Journal of Geophysical Research* 107 (C4), 8687–8705.
- Ross, R.M., Quetin, L.B., Lascara, C.M., 1996a. Distribution of Antarctic krill and dominant zooplankton west of the Antarctic Peninsula. In: Ross, R.M., Hofmann, E.E., Quetin, L.B. (Eds.), *Foundations for Ecological Research West of the Antarctic Peninsula*, Antarctic Research Series 70. AGU, Washington, DC, pp. 199–217.
- Ross, R.M., Hofmann, E.E., Quetin, L.B. (Eds.), 1996b. *Foundations for Ecological Research West of the Antarctic Peninsula*, Antarctic Research Series 70. AGU, Washington, DC, 448pp.
- Sherwin, T.J., 1988. Analysis of an internal tide observed on the Malin Shelf, north of Ireland. *Journal of Physical Oceanography* 18, 1035–1050.
- Sherwin, T.J., Taylor, N.K., 1990. Numerical investigations of linear internal tide generation in the Rockall Trough. *Deep-Sea Research* 37 (10), 1595–1618.
- Simpson, J.H., Rippeth, T., 1993. The Clyde Sea: a model of the seasonal cycle of stratification and mixing. *Estuarine Coastal Shelf Science* 37, 129–144.
- Small, L.F., Menzies, D.W., 1981. Patterns of primary productivity and biomass in a coastal upwelling region. *Deep-Sea Research* 28A, 123–149.
- Smith, D.A., Klinck, J.M., 2002. Water properties on the west Antarctic Peninsula continental shelf: a model study of effects of surface fluxes and sea ice. *Deep-Sea Research II* 49, 4863–4886.
- Smith, D.A., Hofmann, E.E., Klinck, J.M., Lascara, C.M., 1999. Hydrography and circulation of the West Antarctic Peninsula Continental Shelf. *Deep-Sea Research I* 46, 925–949.
- Steele, M., Morison, J.H., Untersteiner, N., 1989. The partition of air–ice–ocean momentum exchange as a function of ice concentration, floe size and draft. *Journal of Geophysical Research* 94 (C9), 12739–12750.
- Stigebrandt, A., 1976. Vertical diffusion driven by internal waves in a sill fjord. *Journal of Physical Oceanography* 6, 486–495.
- Stigebrandt, A., 1999. Baroclinic wave drag and barotropic to baroclinic energy transfer at sills as evidence by tidal retardation, seiche damping and diapycnal mixing in fjords. In: Muller, P., Henderon, D. (Eds.), *Dynamics of Internal Gravity Waves II*, Proceedings of the Aha Huliko‘a Hawaiian Winter Workshop. University of Hawaii, Honolulu, Hawaii, pp. 73–82.
- Stigebrandt, A., Aure, J., 1989. Vertical mixing in basin waters of fjords. *Journal of Physical Oceanography* 19, 917–926.
- Toole, J.M., 1981. Sea ice, winter convection and temperature minimum layer in the Southern Ocean. *Journal of Geophysical Research* 86 (C9), 8037–8047.
- Trenberth, K.E., 1984. Signal versus noise in the southern oscillation. *Monthly Weather Review* 112 (2), 326–332.
- Visbeck, M., Fischer, J., 1995. Sea-surface conditions remotely-sensed by upward-looking ADCPs. *Journal of Atmospheric and Oceanic Technology* 12 (1), 141–149.
- Wallace, M.I., 2007. *Ocean circulation, properties and variability in Marguerite Bay, west Antarctic Peninsula*. Ph.D. Thesis, The Open University, Milton Keynes, UK, unpublished.
- Winant, C.D., 1980. Downwelling over the southern California shelf. *Journal of Physical Oceanography* 10, 791–799.